WWW.OEAW.AC.AT

ÖAW ÖSTERREICHISCHE AKADEMIE DER WISSENSCHAFTEN

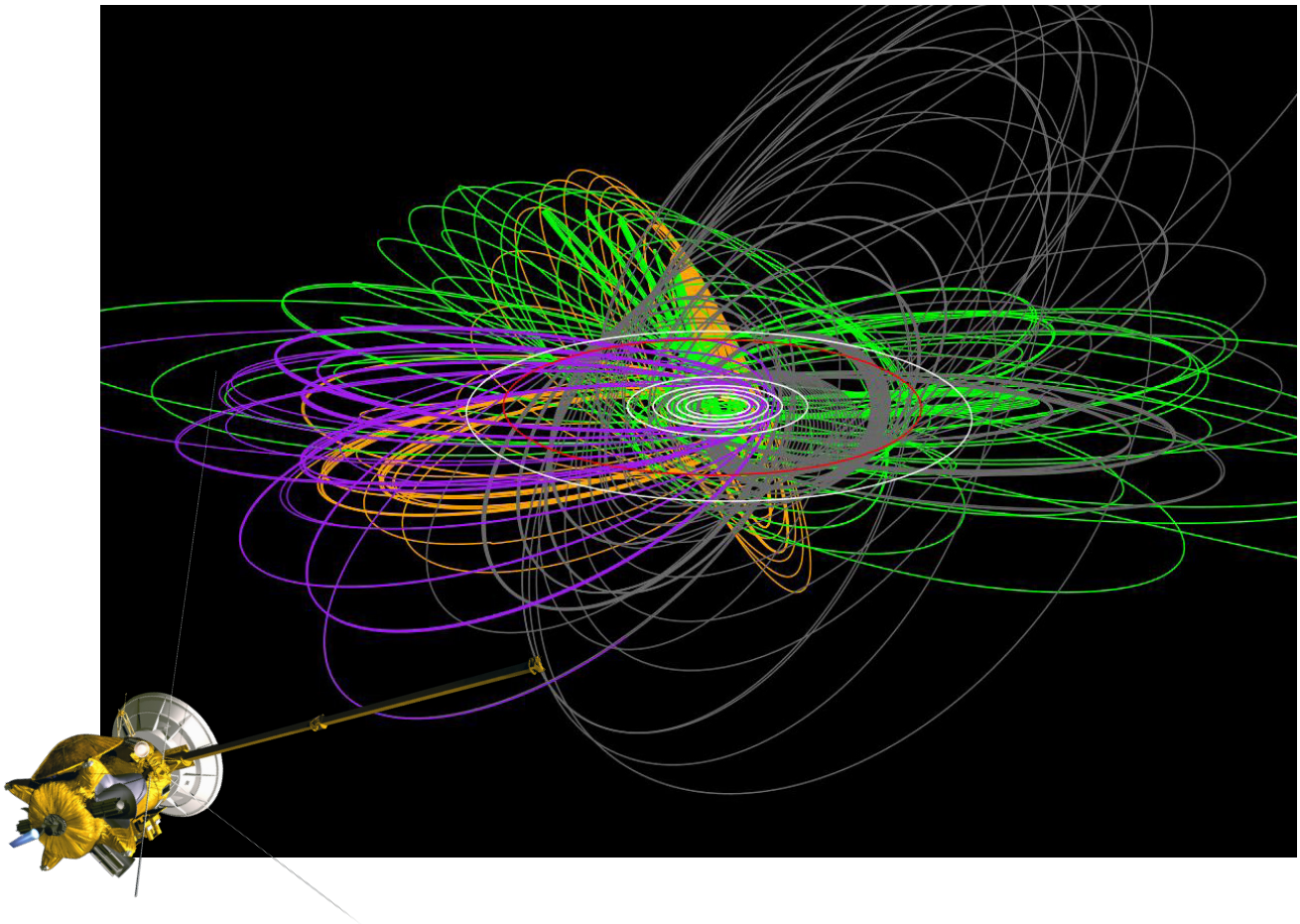

ANNUAL REPORT 2017

IWF INSTITUT FÜR WELTRAUMFORSCHUNG

WWW.IWF.OEAW.AC.AT

ÖSTERREICHISCHE AKADEMIE DER WISSENSCHAFTEN

ANNUAL REPORT 2017

IWF
INSTITUT FÜR WELTRAUMFORSCHUNG

COVER IMAGE

NASA's *Cassini* spacecraft has been on an epic road trip, as this graphic of its orbits around the Saturn system shows. This picture traces *Cassini's* orbits from Saturn orbit insertion in June 2004 through the end of the mission in September 2017. Saturn is in the center, with the orbit of its largest moon Titan in red and the orbits of its six other inner satellites in white. *Cassini's* prime mission is shown in green. Its first mission extension is shown in orange. The completed orbits of its second mission extension are shown in purple. Orbits after *Cassini's* 15th anniversary of launch, on 15 October 2012, appear in dark gray. These include orbits that pass inside Saturn's innermost ring, which started in April 2017 (Credit: NASA/JPL-Caltech).

TABLE OF CONTENTS

INTRODUCTION 5

EARTH & MOON 7

- GRAVITY FIELD 7
- SATELLITE LASER RANGING 9

NEAR-EARTH SPACE 11

SOLAR SYSTEM 17

- SUN & SOLAR WIND 17
- MERCURY 19
- VENUS & MARS 20
- JUPITER & SATURN 22
- COMETS & DUST 24

EXOPLANETARY SYSTEMS 25

INFRASTRUCTURE 29

OUTREACH 31

PUBLICATIONS 33

PERSONNEL 43

IMPRESSUM

INTRODUCTION

The Space Research Institute (Institut für Weltraumforschung, IWF) in Graz focuses on the physics of space plasmas and (exo-)planets. With about 100 staff members from 20 nations (Fig. 1) it is one of the largest institutes of the Austrian Academy of Sciences (Österreichische Akademie der Wissenschaften, ÖAW).

IWF develops and builds space-qualified instruments and analyzes and interprets the data returned by them. Its core expertise is in building magnetometers and on-board computers, as well as in satellite laser ranging, which is performed at a station operated by IWF at the Lustbühel Observatory. In terms of science, the institute concentrates on dynamical processes in space plasma physics, on the upper atmospheres of planets and exoplanets, and on the gravity fields of the Earth and the Moon.

IWF cooperates closely with space agencies all over the world and with numerous other national and international research institutions. A particularly intense cooperation exists with the European Space Agency (ESA).

The institute is currently involved in seventeen active and future international space missions; among these:

- *BepiColombo* will be launched in 2018 to investigate planet Mercury, using two orbiters, one specialized in magnetospheric studies and one in remote sensing.
- ESA's first Small-class mission *CHEOPS (CHaracterizing ExOPlanets Satellite)* will classify exoplanets in detail. Its launch is expected in 2018.
- The *China Seismo-Electromagnetic Satellite (CSES)*, launched in early 2018, studies the Earth's ionosphere.
- ESA's *Cluster* mission still provides unique data leading to a new understanding of space plasmas.
- *GEO-KOMPSAT-2A* is a Korean satellite for space weather investigations due for launch in 2018.
- ESA's *JUpiter ICy moons Explorer (JUICE)* will observe the giant gaseous planet Jupiter and three of its largest moons, Ganymede, Callisto, and Europa. It is planned for launch in 2022.
- *MMS* uses four identically equipped spacecraft to explore the acceleration processes that govern the dynamics of the Earth's magnetosphere.

Fig. 1: Most IWF members in the institute's atrium (Credit: Daniel Hinterramskogler/ÖAW).

- ESA's third Medium-class science mission *PLATO* is a space-based observatory to search for planets orbiting alien stars. It is planned for launch by 2026.
- *Solar Orbiter* is to study along an innovative trajectory solar and heliospheric phenomena, planned for launch in 2020.
- *THEMIS* has been reduced to a near-Earth three-spacecraft mission. The two other spacecraft are now orbiting the Moon in the *ARTEMIS* mission.

HIGHLIGHTS IN 2017

- 15 September marked the end of one of the most successful space missions of the last decades. NASA's *Cassini* mission orbited Saturn for 13 years. Launched in 1997, it reached the ring planet in 2004 and had several hundred close encounters with the gas giant and its moons Titan and Enceladus. IWF participated in more than 50 publications in international journals.
- In "Nature Astronomy" an international team with relevant IWF participation reported the discovery of a sun-type star in a close, eccentric binary system with a neutron star, where the non-degenerate star presents strong Ca-rich pollution from the supernova ejecta.
- A "Nature Communications" study, led by IWF, described how magnetic reconnection in vortices at the magnetopause on the flanks of the magnetotail facilitates turbulent mass transfer into the magnetosphere.
- Induction heating can completely change the energy budget of an exoplanet and even melt its interior. In a study published by "Nature Astronomy" an international team led by IWF with participation of the University of Vienna explained how magma oceans can form under the surface of exoplanets as a result of induction heating.

THE YEAR 2017 IN NUMBERS

Members of the institute published 140 papers in refereed international journals, of which 49 were first author publications. During the same period, articles with authors from the institute were cited 4518 times in the international literature. In addition, 90 talks and 41 posters were presented at international conferences by IWF members. Last but not least, institute members were involved in the organization of three international meetings or workshops.

IWF STRUCTURE AND FUNDING

IWF is structured into four research fields represented by eight research groups (Fig. 2). Wolfgang Baumjohann serves as Director, Werner Magnes as Deputy Director.

The bulk of financial support is provided by ÖAW. Significant support is also given by other national institutions, in particular the Austrian Research Promotion Agency (Österreichische Forschungsförderungsgesellschaft, FFG) and the Austrian Science Fund (Fonds zur Förderung der wissenschaftlichen Forschung, FWF). Furthermore, European institutions like ESA and the European Union contribute substantially.

Fig. 2: IWF group leaders: Y. Narita, H. Lammer, R. Nakamura, W. Magnes, M. Steller, L. Fossati, and N. Kömle (absent: G. Kirchner; Credit: Daniel Hinterramskogler/ÖAW).

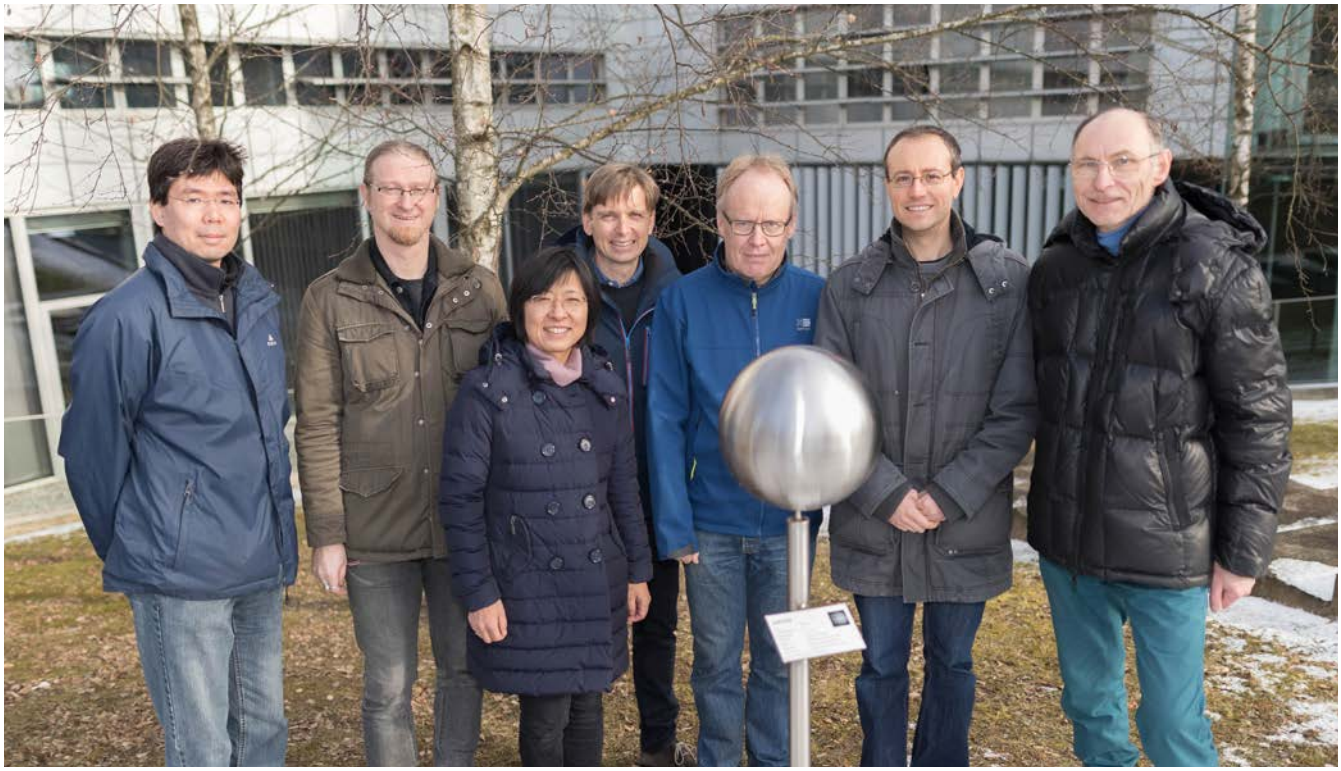

EARTH & MOON

In the last decades, gravimetric and geometric space geodesy techniques constitute an integral part in Earth and planetary sciences. To improve our knowledge about the environment, state and evolution of the Earth and the Earth's only natural satellite, the Moon, IWF is engaged in terrestrial and lunar gravity field research as well as space weather dynamics, and Satellite Laser Ranging to Earth-orbiting satellites and debris objects.

GRAVITY FIELD

Gravity field research includes the analysis of data collected by Earth- and Moon-orbiting spacecraft.

GRAIL

The *Gravity Recovery And Interior Laboratory (GRAIL)* mission aims at answering longstanding questions about Earth's Moon and provides a better understanding of how the Earth and other terrestrial planets were formed. Mapping the structure of the lunar interior gives insight into a variety of geophysical processes, and allows indirectly to shed light on the thermal evolution. The two *GRAIL* spacecraft were orbiting the Moon in nearly circular polar orbits at an average altitude of 55 km during the primary mission phase. As the distance between the two probes changed slightly due to different gravity induced perturbations, the inter-satellite range variations were recorded by means of Ka-band observations. Hence, this type of observations is ideally suited to reveal the lunar gravity field (even at the far side) with unprecedented accuracy.

IWF released the first completely independent and most accurate lunar gravity model, based on *GRAIL* mission data, outside the United States of America - denoted as GrazLGM420b. The model is resolved up to spherical harmonic degree 420, which corresponds to a spatial resolution of around 13 km (see Fig. 3).

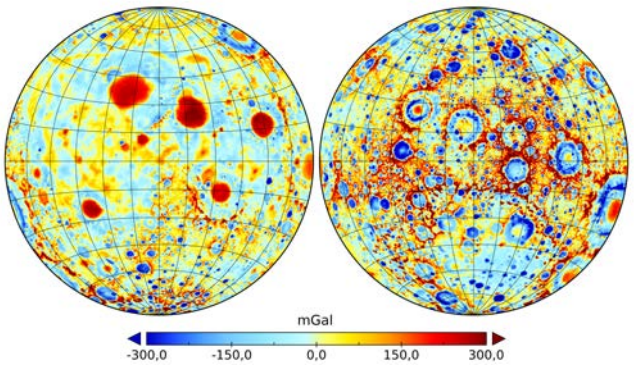

Fig. 3: Lunar gravity model GrazLGM420b in terms of gravity anomalies with the nearside on the left and the far side on the right.

The reconstruction of an independent gravity field solution requires absolute position information of the satellites. Hitherto, lunar gravity models compiled in Europe relied so far on the orbit products provided by the *GRAIL* Science Team. However, Doppler observations collected by the Deep Space Network (DSN) on Earth allows for determining the *GRAIL* orbits. Through the development of the in-house software package ORCA (Orbit Re-Construction Application) the opportunity was opened to infer the positions of the *GRAIL* probes based on S-band radiometric tracking data collected by the DSN. Based on an iterative process, which initially utilizes a pre-*GRAIL* gravity field as starting point, a final independent solution was created. The nominal accuracy of radiometric 2-way S-band observations to *GRAIL* is estimated to be 1 mm/s.

Though, the achieved accuracy exceeds the assumptions and is in the range of 0.04 - 0.5 mm/s. Fig. 4 shows the obtained a posteriori fit to the S-band DSN data corresponding to 0.12 mm/s on average. According to the *GRAIL* Science Team the posteriori fit is around 0.13 mm/s, which indicates a good agreement to our precise orbit determination solution.

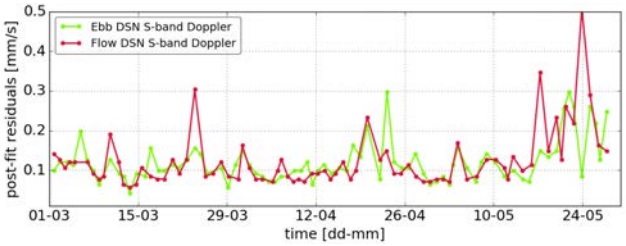

Fig. 4: Postfit residuals in the form of root mean square (RMS) from S-band DSN data to GRAIL using GrazLGM420b.

GRACE

The year 2017 marked the end of the scientific operations of the highly successful twin-satellite mission *GRACE* (*Gravity Recovery And Climate Experiment*, NASA/DLR). For more than 15 years, *GRACE* has provided time-variable gravity field information with unprecedented accuracy which substantially contributed to a better understanding of how mass is constantly being redistributed around the Earth. This information is of utmost importance, not only for geophysicists, but also for any researcher studying the effects of global climate change. In this context, a particularly crucial application of *GRACE* resides in the possibility to directly monitor changes in the Earth's cryosphere, i.e., glaciers, ice caps and ice sheets. Besides the thermal expansion of ocean water, presently glacier shrinkage has been identified as the most dominant contributor to global sea level rise.

In the framework of the IWF-led project *SPICE*, a sophisticated analysis approach has been developed to deduce reliable estimates of mass balances of alpine glacier systems (Alps, Alaska, Iceland, Svalbard etc.) from space-gravimetric data. The innovative methodology approximates the regional gravity field in the vicinity of the investigated glaciers with radial basis functions (point masses) and exploits *GRACE* on the level of raw inter-satellite measurements (Level-1B). To stabilize the (naturally ill-posed) gravity inversion, Tikhonov regularization is applied. The selection of an appropriate regularization parameter is done in an exceptional way: the extended Gauss-Markov model is regarded as a multi-objective optimization problem, which is solved by utilizing stochastic optimization methods (Genetic Algorithms). These three measures, as opposed to the typically applied (global) spherical harmonics modeling (Fig. 5; blue curve), ensure the best possible regionalization of both modeling and data and consequently prevent the solutions from being oversmoothed.

GRACE data have been processed and provided by the project partners at TU Graz. Isolation of the glaciological signal is made more reliable by using both global and regional hydrological models. The final glacier mass balance estimates, based on a novel point mass approach (PM), are validated by comparison with in-situ observations provided by the World Glacier Monitoring Service (WGMS) in Zurich (Fig. 5; red and black curve, respectively).

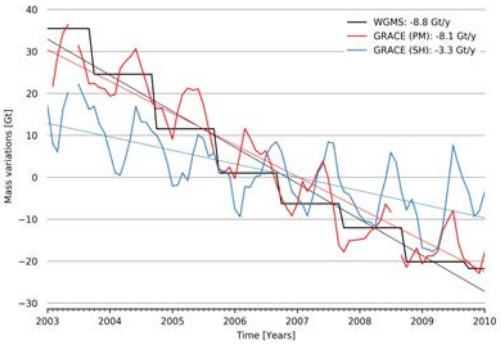

Fig. 5: Viability of the presented novel method for the example of Iceland.

SPACE WEATHER APPLICATIONS

Dedicated gravity field missions like *GRACE* or its successor *GRACE* Follow-on (launch date: March 2018) measure all forces acting on a spacecraft to recover the Earth's gravity field. A core instrument aboard this kind of satellites are accelerometers, which enable the measurement of the non-gravitational part of the perturbing forces. In addition to the substantial benefit for the gravity field research, these instruments also allow the determination of time-variable atmospheric mass densities along the satellite trajectory. Since space weather disturbances can affect spaceborne and ground based technologies, the knowledge of the current state of the thermosphere is very important.

For this reason, the impact of nearly 400 solar events on the Earth's thermosphere and the magnetic field in the interplanetary medium have been thoroughly analyzed. The events, which occurred between 2003 and 2015, included 196 coronal mass ejections (CMEs) and 195 corotating interactions regions (CIRs). Atmospheric mass densities have been estimated by means of *GRACE* accelerometer measurements and Bz magnetic field component variations were observed by the *Advanced Composition Explorer (ACE)* satellite, located at the Lagrange point 1 (L1). Thereby, a strong causal link between these two types of observations could be deduced (see Fig. 6). Hence, this comprehensive study provides a solid basis for a future forecasting tool to estimate the expected impact of a solar event on the Earth's thermosphere based on near real-time observations of the Bz component at L1.

In today's modern society, with the steadily increasing technology, these activities show that IWF is aware of the necessity to recognize and face up to the space weather threat.

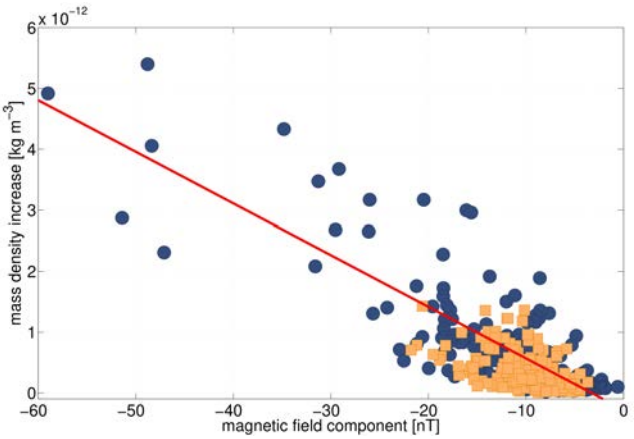

Fig. 6: Scatter plot of the Bz component *(ACE)* vs. the increase in the neutral density *(GRACE)*. The analyzed CME and CIR events are marked with blue circles and orange squares, respectively.

SATELLITE LASER RANGING

In addition to routinely tracking more than 150 targets which are equipped with laser retro-reflectors, the Graz Satellite Laser Ranging (SLR) Station is working on various projects. Highlights include the founding of a space debris expert center, polarization switching measurements to *Galileo* satellites and quantum key distribution experiments in cooperation with the ÖAW Institute for Quantum Optics and Quantum Information (IQOQI) Vienna.

QUANTUM KEY DISTRIBUTION

With the growth of internet use and electronic commerce, a secure global network for data protection is desirable. A drawback of traditional public key cryptography is that it is not possible to guarantee information security. However, quantum key distribution (QKD) offers unconditional security ensured by the laws of physics. QKD uses the fundamental unit of light, single photons, encoded in quantum superposition states, which are sent to distant locations. By proper encoding and decoding, two distant parties share strings of random bits called secret keys.

In a collaborative project between the Austrian and Chinese Academies of Sciences and the University of Vienna, intercontinental QKD has been demonstrated for the very first time in 2017 between ground stations in Austria and China. Therefore, the Graz SLR Station at Lustbühel Observatory was equipped with a dedicated quantum detection package developed by IQOQI. This allowed detecting and analyzing the polarization state of the single photon signal transmitted from the Chinese Low Earth Orbit satellite *Micius*. Furthermore, using the satellite as a trusted relay station, secure quantum keys could be exchanged with the Xinglong and Nanshan ground stations in China. These keys were then used for intercontinental quantum-secured communication by transmitting images in a one-time pad configuration as well as a video conference between Austria and China. Fig. 7 shows a long-term exposure picture of the SLR station while tracking the Chinese Satellite.

Fig. 7: The Graz SLR Station at Lustbühel Observatory tracking the Chinese satellite *Micius* in a long-term exposure picture. One can see the red uplink as well as the green downlink beacon lasers.

EXPERT COORDINATION CENTER

With ESA's Space Situational Awareness program an Expert Coordination Centre was founded at ESOC, Darmstadt. A consortium was formed consisting of experts for optical observations (Astronomical Institute of Bern, Czech Technical University in Prague, SpaceDys) and space debris laser ranging (Graz SLR Station). The Expert Center's main task is to coordinate external stations, in terms of observation scheduling/tasking and data delivery. Furthermore, within the framework of the project several data conversion tools were developed.

The Graz SLR Station developed an acceptance process for SLR candidate stations to become a "qualified" space debris laser ranging station according to pre-defined criteria. The acceptance process was split into three parts. 1) Validation: The candidate sensor has to measure a number of full passes to targets with well-known orbits (e.g. *Lageos-1*/*Lageos-2*) using a space debris laser. The results are compared to the *Lageos* ILRS reference orbit by applying a validation routine. 2) Qualification: Within the qualification campaign the candidate sensor has to deliver the results of at least three successful observation sessions performing measurements to arbitrary space debris targets. The station has to reach certain success criteria to pass to the next phase. 3) Dedicated campaign: According to a fixed target priority list the station has to deliver a certain amount of passes within a month's time.

The functionality of the acceptance process was demonstrated successfully for the SLR station in Borówiec, Poland, delivering space debris laser ranging data to *Lageos 1* (Fig. 8) and *Lageos 2*.

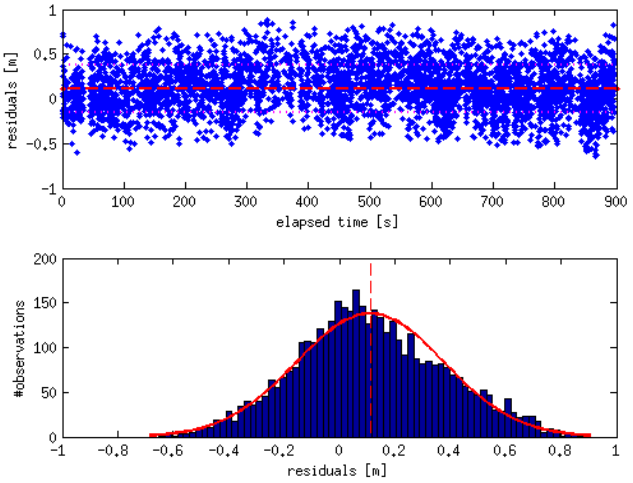

Fig. 8: Space debris laser ranging residuals [m] over time [s] to *Lageos 1* for Borówiec SLR station (top). The histogram analysis of the range residuals to *Lageos 1* showed a range bias of 0.1 m in comparison with the ILRS reference orbit (bottom).

SPACE DEBRIS OBSERVATIONS

The upper stage of the Long March 3B rocket body (NORAD ID: 38253) reentered the Earth's atmosphere in August 2017. One month before reentry, light curves (Fig. 9; white) were recorded by using single photon avalanche diodes while simultaneously doing distance measurements via space debris laser ranging (Fig. 9; green). The light curve measurements were taken using the reflected sunlight of the satellite gathered by our receiving telescope with wavelengths other than the 532 nm (which is used for SLR). Space debris laser ranging was performed with a high power laser operating at 20 W / 100 Hz.

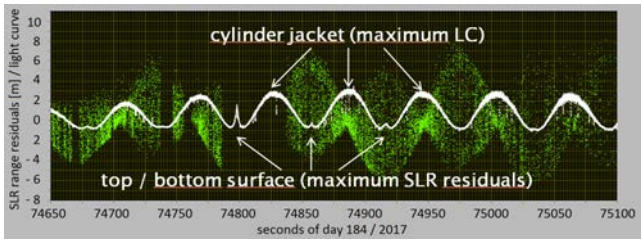

Fig. 9: Space debris laser ranging range residuals (white, in meters) and light curve measurements (green, proportional to the number of single photon returns within 10 ms intervals) vs. the seconds of day. The light curve is scaled accordingly to fit within the plot of the range residuals.

The simplified shape of the rocket body can be assumed to be cylindrical, with a height of 12.38 m and a diameter of 3 m. Within a single pass of the rocket body it is possible to draw conclusions on the orientation of the space debris part. Since both data sets are oscillating, it implies that the rocket body is rotating – with a rotation period of about 120 s.

The maximum offset of the SLR range residuals is about 12 m, which corresponds well to the rocket body dimensions. This implies that the cylinder symmetry axis is oriented close to the observer's line of sight. Furthermore, the SLR maxima are aligned with the small and sharp light curve peaks. These arise from the reflection of the sunlight on the top/bottom surface of the rocket body.

At the minimal SLR residuals the light curve shows a broad reflection maximum. These peaks are related to sunlight reflections of the cylinder jacket. The cylinder symmetry axis is hence lying within a plane normal to the line of sight of the observer.

Based on a cylindrical model of the rocket body simulated light curves and SLR residuals were calculated along the path by using Simplified General Perturbations (SGP4) orbit propagation. The modeled cylinder was rotated along the path using the period from the measured light curve and the SLR data. Different starting conditions regarding the orientation of the cylinder axis and the starting phase angle were simulated. A comparison of experimental results with the simulations allowed to draw conclusions on the rotation parameters of the rocket body with respect to the Earth centered inertial system.

ALCANTARA INITIATIVE

ESA's Alcantara Initiative is a program to build bridges between international research partners by sharing their knowledge. Within this initiative a project was conducted in cooperation with the Argentine-German Geodetic Observatory. SLR measurements to *Galileo* satellites were performed continuously over up to four hours. During this time, the polarization state of the outgoing laser beam was switched, in intervals of one minute, between linear polarization along track, across track and circular polarization. In total 15 *Galileo* passes were analyzed regarding laser polarization induced offsets of the range measurements.

In previous studies systematic offsets have been found for retro-reflector arrays of older *Glonass* satellites. These offsets are connected to fabrication errors of the corner cube retro-reflectors shifting the mean reflection point millimeters towards or away from the observing station. The goal of the present study was to investigate if *Galileo* reflector panels show similar effects. The current *Galileo* reflector panels do not show systematics, the offsets between the range residuals of different polarization states (polarization offset [mm]) are distributed evenly around zero (Fig. 10). The RMS of the polarization offset increases for lower elevations (corresponding to a larger incidence angle on the retro-reflector panel). Comparing adjacent measurements of the same polarization state does not show this elevation dependent effect. Thus, the effect was explained by the superposition of the far field diffraction patterns of differently "clocked" (rotated) retro-reflectors on the *Galileo* retro-reflector panel. Depending on the incident angle of the laser beam on the panel polarization-based offsets occur.

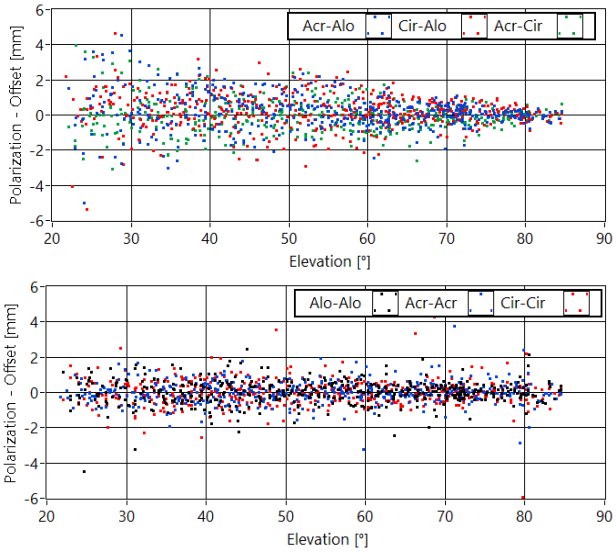

Fig. 10: Polarization offsets [mm] between different polarizations (top; Alo = along track, Acr = across track, Cir = circular) and between adjacent measurements of the same polarization (bottom) plotted against the satellite elevation [°].

NEAR-EARTH SPACE

Near-Earth space is a most suitable place to study fundamental space plasma processes due to recent advancements in the in-situ measurements of the charged particles together with electric and magnetic fields at high cadence. IWF has been participating in the hardware activities of numerous missions, now operating, being built as well as in the planning phase. Data taken from these missions have been extensively analyzed at IWF by applying different analysis methods to the data and by theoretical modeling to compare with the observations. The obtained knowledge contributes to the better understanding of different processes in space plasma applicable to those in our solar system and beyond.

CLUSTER

The *Cluster* spacecraft have been providing data since 2001 as the first four spacecraft mission in space for studying small-scale structures of the Earth's magnetosphere and its environment. The mission is currently planned to be extended to December 2018. IWF is PI/Co-I on five instruments and has maintained the *Austrian Cluster Data Center*. In addition to data analysis, IWF contributed to data archiving activities at the *Cluster Science Archives (CSA)* by also producing supporting data products such as science event lists.

MMS

NASA's *MMS (Magnetospheric MultiScale)* mission, launched in 2015, explores the dynamics of the Earth's magnetosphere and its underlying energy transfer processes. Four identically equipped spacecraft carry out measurements with high temporal and spatial resolution. *MMS* investigates the small-scale basic plasma processes, which transport, accelerate and energize plasmas in thin boundary and current layers. The *MMS* orbit of the first two years was dedicated to study dayside magnetopause reconnection. In mid 2017, the apogee was raised to encounter near-Earth magnetotail reconnection.

IWF, which is the biggest non-US participant in *MMS*, has taken the lead for the spacecraft potential control of the satellites *(ASPOC)* and is participating in the electron drift instrument *(EDI)* and the digital fluxgate magnetometer *(DFG)*. In addition to the operation activities of these instruments and scientific data analysis, IWF is contributing to develop new methods of inflight calibration and an algorithm to produce new science data products.

THEMIS/ARTEMIS

NASA's *THEMIS* mission, launched in 2007, consisted of five identical satellites flying through different regions of the magnetosphere. In autumn 2010 the two outer spacecraft became *ARTEMIS* in orbit around the Moon, while the other three *THEMIS* spacecraft remained in their orbit. As Co-I of the magnetometer, IWF is participating in processing and analyzing data.

EFFECT OF ELECTRIC FIELDS ON SPACECRAFT POTENTIAL

It has been a puzzle since the early days of the *Cluster* mission why the spacecraft potential - despite being limited by the ion beam emitted by the *ASPOC* instrument - sometimes exhibits spikes, which are higher than any variation of the ambient plasma could induce. The high-resolution *MMS* data revealed a clear correlation - with squared regression coefficients better than 0.8 - between the spacecraft potential (center panel of example in Fig. 11) and the ambient electric field (bottom panel) whereby a field of the order of 10 mV/m may already increase the potential by one volt. In comparison, the variation of the plasma electron current to the spacecraft surface (top panel) by a factor of 2 causes no significant reaction of the potential.

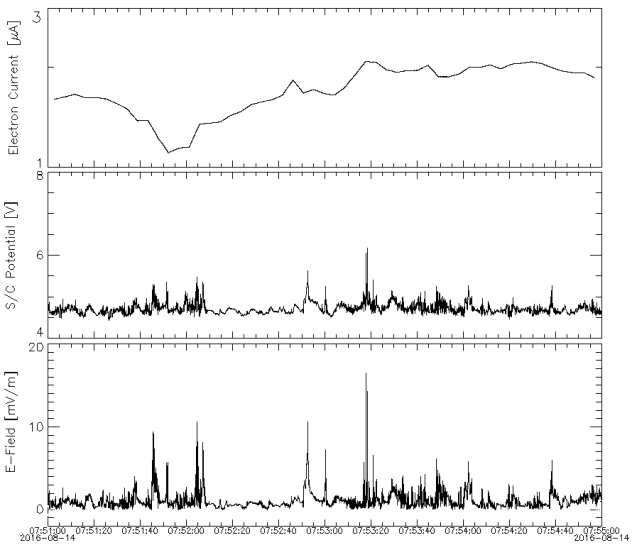

Fig. 11: Electron current deduced from plasma instrument (top); spacecraft potential (middle:); electric field obtained from double probe measurement aboard *MMS* during an interval when *ASPOC* was operating (bottom).

After removal of the electric field effect, the spacecraft potential becomes a much more accurate indicator of plasma density. The interpretation is subject to ongoing studies and numerical simulations. Most likely, the effect is related to the size of the spacecraft together with its long conductive wire booms (~120 m tip to tip), which form a huge equipotential structure. Due to the electric field, the potential of the body relative to the ambient plasma is no longer a single value but depends on the position. The resulting asymmetry of the sheath around the spacecraft body impedes the return of photo-electrons to the body. This in turn enforces an increase of the spacecraft potential to maintain the equilibrium of currents. The same mechanism should affect the spacecraft potential when *ASPOC* is not operating, but may be hidden behind stronger variations due to the ambient plasma.

CSES

The *China Seismo-Electromagnetic Satellite (CSES)* mission was launched in early 2018. It will be the first Chinese platform for the investigation of natural electromagnetic phenomena with major emphasis on earthquake monitoring from a Sun synchronous, polar, Low Earth Orbit (LEO).

The *CSES* magnetometer was developed in cooperation between the National Space Science Center (NSSC) of the Chinese Academy of Sciences, the Institute of Experimental Physics (IEP) of TU Graz, and IWF. NSSC is responsible for the dual sensor fluxgate magnetometer, the instrument processor and the power supply unit, while IWF and IEP participate with the newly developed absolute scalar magnetometer, called *Coupled Dark State Magnetometer (CDSM)*. In 2017, the *CDSM* Flight Model was delivered to China, integrated onto the spacecraft and accepted for flight (Fig. 12).

Fig. 12: *CSES* team from IWF and Graz University of Technology (TU Graz) ready to launch the *CDSM* magnetometer.

GEO-KOMPSAT-2A

GEO-KOMPSAT-2 (Geostationary Korea Multi-Purpose Satellite-2) consists of two spacecraft, which are built and managed by the South Korean Space Agency KARI. Both satellites focus on meteorological survey measurements from a geostationary orbit above Korea. One of the spacecraft, *GEO-KOMPSAT-2A (GK-2A)*, carries additional instrumentation to investigate space weather phenomena.

In cooperation with ESA and international partners, IWF is engaged in *GK-2A* with a four-sensor magnetometer called *Service Oriented Spacecraft MAG-netometer (SOSMAG)*. It was developed with ESA technology grants and serves as a ready-to-use space weather monitoring system to be mounted on a variety of different spacecraft built without a magnetic cleanliness program. Up to two high-resolution boom-mounted fluxgate magnetometers, the Digital Processing Unit (DPU) and the boom are provided by Magson GmbH and Technische Universität Braunschweig. For detection and characterization of magnetic disturbers on the spacecraft, two magnetometers based on the anisotropic magnetoresistive (AMR) effect were developed in a joint effort by Imperial College London and IWF (see AMR front-end electronics in Fig. 13).

In 2017, the flight model of *SOSMAG* was assembled, calibrated, acceptance tested, delivered to South Korea and integrated onto the *GK-2A* spacecraft as part of the *Korean Space Environment Monitor (KSEM)* instrument suit. It will be launched in early 2019.

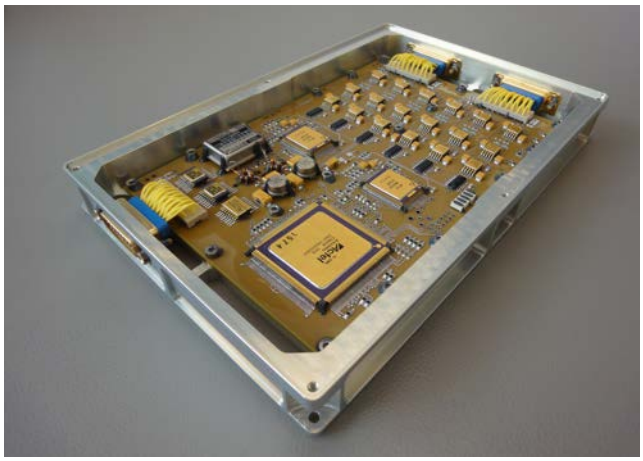

Fig. 13: Flight electronics of the two AMR sensors.

SMILE

The *Solar wind Magnetosphere Ionosphere Link Explorer (SMILE)* is a joint mission between ESA and the Chinese Academy of Sciences. It aims to build a more complete understanding of the Sun-Earth connection by measuring the solar wind and its dynamic interaction with the magnetosphere. IWF is Co-Investigator for two instruments: the *Soft X-ray Imager (SXI)* and the magnetometer *(MAG)*.

MAGNETOMETER OFFSET DETERMINED FROM COMPRESSIONAL WAVES

Magnetometers on-board spacecraft need to be regularly calibrated in flight. In low fields, the most important calibration parameters are the three offset vector components, which represent the magnetometer measurements in vanishing ambient magnetic fields. A new method has been developed to determine these three components from magnetic field measurements of highly compressional waves, e.g., mirror modes in the Earth's magnetosheath. Correspondingly, the method is called 3D mirror mode method. Although it shares the same basic working principles with the 1D mirror mode method for spin-axis stabilized spacecraft, it is a completely new development, focused on the calibration of magnetometers on board three-axis stabilized spacecraft.

The method has been tested by applying it to magnetic field data measured by the *THEMIS-C* spacecraft in the terrestrial magnetosheath, the *Cassini* spacecraft in the Jovian magnetosheath, and the *Rosetta* spacecraft in the vicinity of comet 67P/Churyumov–Gerasimenko. The tests reveal that the achievable offset accuracies depend on the ambient magnetic field strength (lower strength meaning higher accuracy), on the length of the underlying data interval (more data meaning higher accuracy) and on the stability of the offset that is to be determined. The method is expected to be applied to the magnetometer data from the *SMILE* spacecraft.

PHYSICS

Data from ongoing missions are analyzed and theoretical models are developed to describe the physical processes in near-Earth space. In particular, high-resolution data from *MMS* enabled a number of new studies dealing with interactions between the solar wind and the magnetosphere, internal disturbances in the magnetosphere such as plasma flows, waves, and plasma instabilities including magnetic reconnection and their large-scale consequences.

EARTH'S MAGNETOPAUSE

The magnetopause is the magnetic barrier that deflects the solar wind plasma and confines the Earth's magnetic field. Data from *MMS* are combined to demonstrate how the plasma and magnetic forces at the boundary affect the interaction between the shocked solar wind and the Earth's magnetic field. These forces with the plasma pressure are examined together with the electron distribution function. Sublayers with thickness compared to the ion scale are found. There are also small pockets of low magnetic field strength, of small radius of curvature, and of high electric current that mark the electron diffusion region. The flow of electrons, parallel and antiparallel to the magnetic field reveals a complex topology with the creation of magnetic ropes at the boundary.

MAGNETOSHEATH HIGH-SPEED JETS

MMS measurements have enabled, for the first time, the study of the rich internal structure of a magnetosheath high-speed jet. Large-amplitude density, temperature, and magnetic field variations inside the jet are revealed. The propagation velocity and normal direction of planar magnetic field structures (i.e., current sheets and waves) have been investigated via four-spacecraft timing. These structures mainly convect with the jet plasma. In the particular jet studied, there are indications of the presence of a tangential discontinuity. At other times, there are small cross-structure flows. Where this is the case, current sheets and waves overtake the plasma in the jet's core region. Ahead and behind that core region, along the jet's path, current sheets are overtaken by the plasma.

Jet structures are found to be mainly thermal and magnetic pressure balance structures, notwithstanding that the dynamic pressure dominates by far. Although the jet is supermagnetosonic in the Earth's frame of reference, it is submagnetosonic with respect to the plasma ahead. Consequently, there is no fast shock. Instead, some evidence is found for (a series of) jets pushing ambient plasma out of their way, thereby stirring the magnetosheath and causing anomalous sunward flows in the subsolar magnetosheath (Fig. 14 A). Furthermore, jets are found to modify the magnetic field in the magnetosheath, aligning it with their propagation direction (Fig. 14 B).

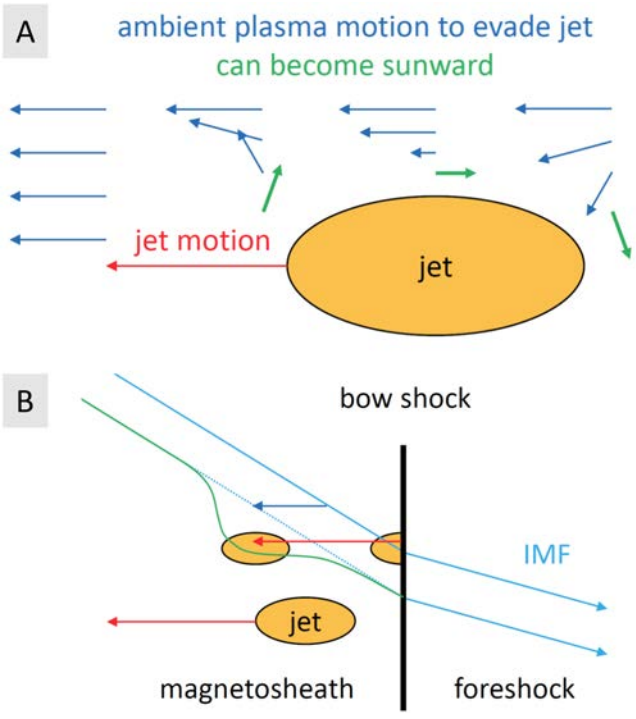

Fig. 14: A: Illustration showing the motion of the magnetosheath plasma (blue and green arrows) in the vicinity of a jet; B: Illustration of how the plasma motion of a jet (red arrow) through slower ambient plasma (blue arrow) modifies the magnetic field in the magnetosheath (green line).

GUIDE FIELD EFFECT ON LOCAL ENERGY CONVERSION DURING ASYMMETRIC MAGNETIC RECONNECTION

MMS data were used to investigate small-scale regions where plasma electron dynamics support the splitting and interconnection of the Earth's magnetic field and the shocked solar wind. Magnetic reconnection can create hazardous energetic particle radiation in near-Earth space by dissipating magnetic energy and accelerating nearby plasma particles. A number of cases were examined, where *MMS* observed reconnection in situ, in order to investigate the nature of the dissipation region.

The results of the study, which are summarized in Fig. 15, indicated that the location of - and mechanism for - dissipation are partially controlled by the angle between the Earth's and the Sun's magnetic fields. During reconnection with high magnetic shear, dissipation is associated with highly agyrotropic meandering electrons near the inner boundary of the reconnection region, the electron flow stagnation point. For very low shear, dissipation is associated with streaming solar wind electrons near the exact site of reconnection, the magnetic X point. For moderate shear, both mechanisms are active.

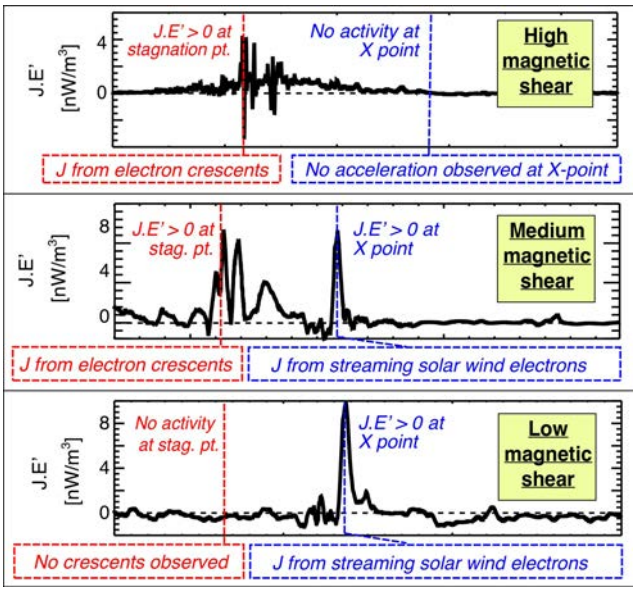

Fig. 15: The dissipation measure (J.E') as a function of time for three typical reconnection sites observed by *MMS*. The top, middle, and bottom plots show reconnection events with very high, moderate, and very low magnetic shear. The vertical red line indicates the time when the electron flow stagnation point was observed. The blue vertical line indicates the time when the magnetic X point was observed. The red and blue boxes describe the source of the current, J, that was associated with the dissipation measure, J.E'.

TURBULENT MASS TRANSFER CAUSED BY VORTEX-INDUCED RECONNECTION IN MAGNETOSPHERIC PLASMAS

Magnetic reconnection is believed to be the main driver to transport solar wind into the Earth's magnetosphere when the magnetopause features a large magnetic shear. However, even when the magnetic shear is too small for spontaneous reconnection, the Kelvin-Helmholtz instability (KHI) driven by a super-Alfvénic velocity shear is expected to facilitate the transport. Although previous kinetic simulations have demonstrated that the non-linear vortex flows from the KHI gives rise to vortex-induced reconnection (VIR) and resulting plasma transport, the system sizes of these simulations were too small to allow the VIR to evolve much beyond the electron-scale as recently observed by the *MMS* spacecraft.

In this study, based on a large-scale fully kinetic simulation (Fig. 16 a) and its comparison with *MMS* observations (Fig. 16 b and c), it is shown for the first time that ion-scale VIR jets rapidly decay through self-generated turbulence (Fig. 16 a), leading to a mass transfer rate nearly one-order higher than previous expectations for the KHI.

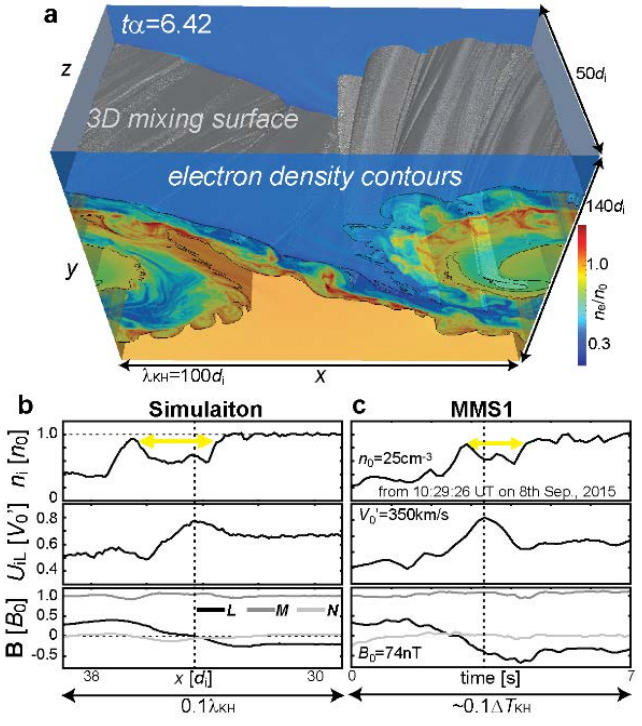

Fig. 16: a) 3D view of mixing surfaces with electron density contours in the x-y planes at z=0 (=L_z) in a non-linear growth phase of the KHI ($t\alpha$=6.42). (b, c) Virtual observation plots for the crossing of an ion-scale VIR jet (b) and in-situ observations by the *MMS1* spacecraft for a 7s interval from 10:29:26 UT on 8 Sep. 2015 (c) of ion density n_i, ion bulk velocity along the jet U_{iL} and magnetic field B. Quantitative consistencies between simulation and observation can be seen especially in the ion jet (enhanced U_{iL}) with a density dip (marked by yellow) during the crossing of the current sheet (B_L change).

REMOTE OBSERVATIONS OF INTENSE RECONNECTION IN THE NEAR-EARTH MAGNETOTAIL

Although the consequences of magnetic reconnection can be detected in a large region in the magnetotail, the spatial and temporal evolution of magnetic reconnection is not well understood due to its localized and transient nature. Uncertainties in identifying the characteristics of the reconnection regions have significantly improved based on remote observations of reconnection by *MMS* combined with *DMSP (Defense Meteorological Satellite Program)* observations from the low Earth orbit during a storm-time substorm on 23 June 2015. The energy and pitch-angle dependent signatures of ions and electrons from these spacecraft have been used to determine the location of the source region, i.e. the reconnection sites.

The high-resolution measurements by *MMS* succeeded in detecting for the first time the dispersion of the electrons together with the ions. The dispersion analysis is shown in Fig 17. The identified location of the reconnection was at 16-18 R_E, which is consistent with that inferred from low Earth orbit *MMS*. The results from detailed analysis from *MMS* indicated also that the underlying magnetotail magnetic reconnection process was intrinsically impulsive during this active X-line event.

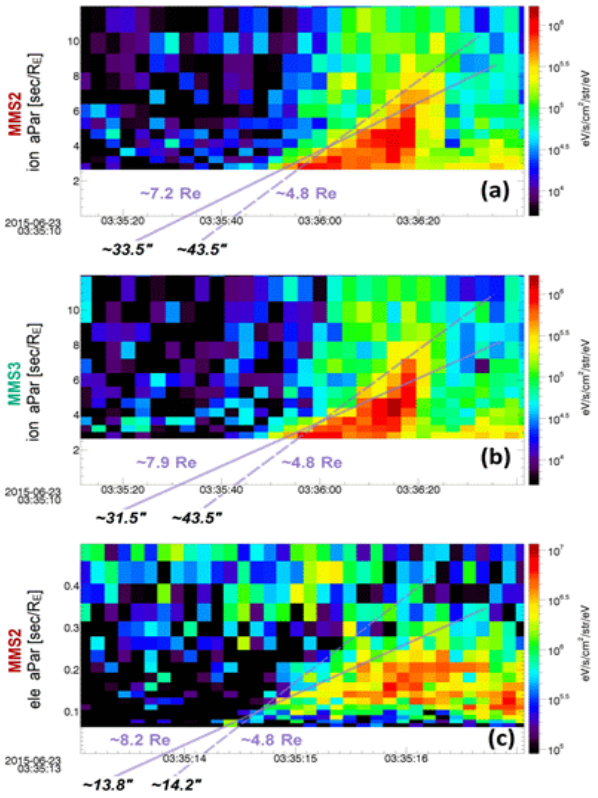

Fig. 17: Energy flux of the anti-field-aligned ions (Earthwards) measured by (a) *MMS2* and (b) *MMS3* spacecraft and electrons from *MMS2* (c). The two purple lines demonstrate the minimum and maximum slope of the dispersion. The estimated maximum distance and the injection times are labeled at the bottom end of the slopes.

LARGE-SCALE DISTURBANCES IN THE MAGNETOTAIL PRODUCED BY A RECONNECTION JET

Although reconnection takes place in a localized region, it creates fast plasma flows, which lead to large-scale disturbances in the near-Earth magnetotail, in particular during a substorm. To study the chain of processes, it is essential to combine *MMS* observations with those of other spacecraft distributed in the magnetosphere. The evolution of the near-Earth plasma sheet during an intense substorm was studied based on multi-point analysis using the measurements from *MMS*, *Geotail*, *GOES*, and *Cluster*, and comparison with an MHD model of the reconnection jet.

Large-scale configuration changes in the magnetotail during a substorm were observed (Fig. 18 left panel) when a number of spacecraft was located in the near-Earth magnetotail (Fig. 18 upper right panel). The spatial structure of the high-speed plasma flows and associated field-aligned current pattern were deduced. These disturbances were compared with an MHD simulation (Fig. 18 lower right panel). It is found that the dynamics in the boundary region of the near-Earth plasma sheet is controlled both by the Earthward flow braking process and by the accumulated magnetic flux due to near-Earth reconnection evolving tailward.

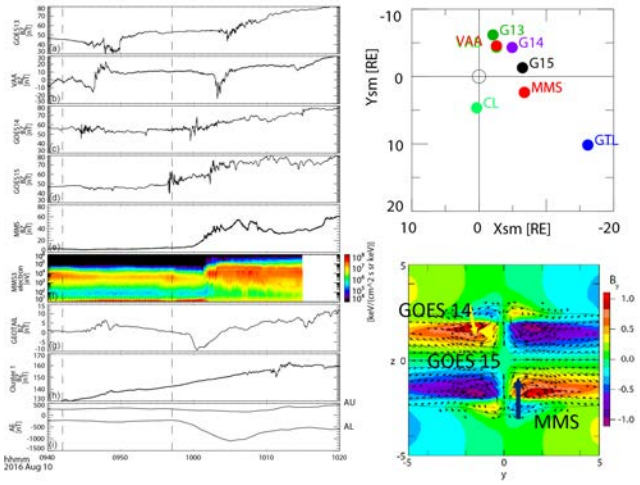

Fig. 18: Magnetic field component normal to the current sheet (BZ) from seven spacecraft: *GOES 13*, *Van Allen Probe-A*, *GOES 14*, *GOES 15*, *MMS3*, *Geotail*, *Cluster 1*, together with electron energy spectra from *MMS1* and *MMS3* and auroral electrojet indices (left panel); spacecraft location in equatorial plane (upper right panel); color-coded By disturbances around the reconnection jets from the MHD simulation. *MMS* and *GOES 14-15* observed disturbances similar to those at the location indicated by arrows (lower right panel).

CATALOG OF ELECTRON VELOCITIES IN THE EARTH'S MAGNETOTAIL

The computation of electron velocity distribution functions in the Earth's magnetotail requires a very large number of particles in order to get a good statistical significance and low noise. Such distributions have recently been observed with the *MMS* mission. The comparison of the simulation results with the observed distributions, when flying through a reconnection region in the Earth's magnetosphere, will foster future research and understanding of reconnection physics. Observers need to know, where in a reconnection region the spacecraft have recorded the data, which cannot be known directly. The comparison to a catalog of predicted electron distribution functions allows to reconstruct the spacecraft trajectory through the magnetotail. In an effort to generate a comprehensive catalog with different plasma conditions, as a first step, an anti-parallel magnetic field case was computed. Samples of highly complex distributions are shown in Fig. 19. The origin of these highly structured distributions still needs to be explained better from reconnection physics.

Fig. 19: Catalog of electron velocity distributions as obtained from 2D particle-in-cell simulations. Each row shows a specific location in the magnetic reconnection region that is similar to the tail (night-side) of the magnetic field of Earth. The maximum probability to find an electron with the given velocities is colored in red, the minimum in blue. The background magnetic field direction is indicated with a green line.

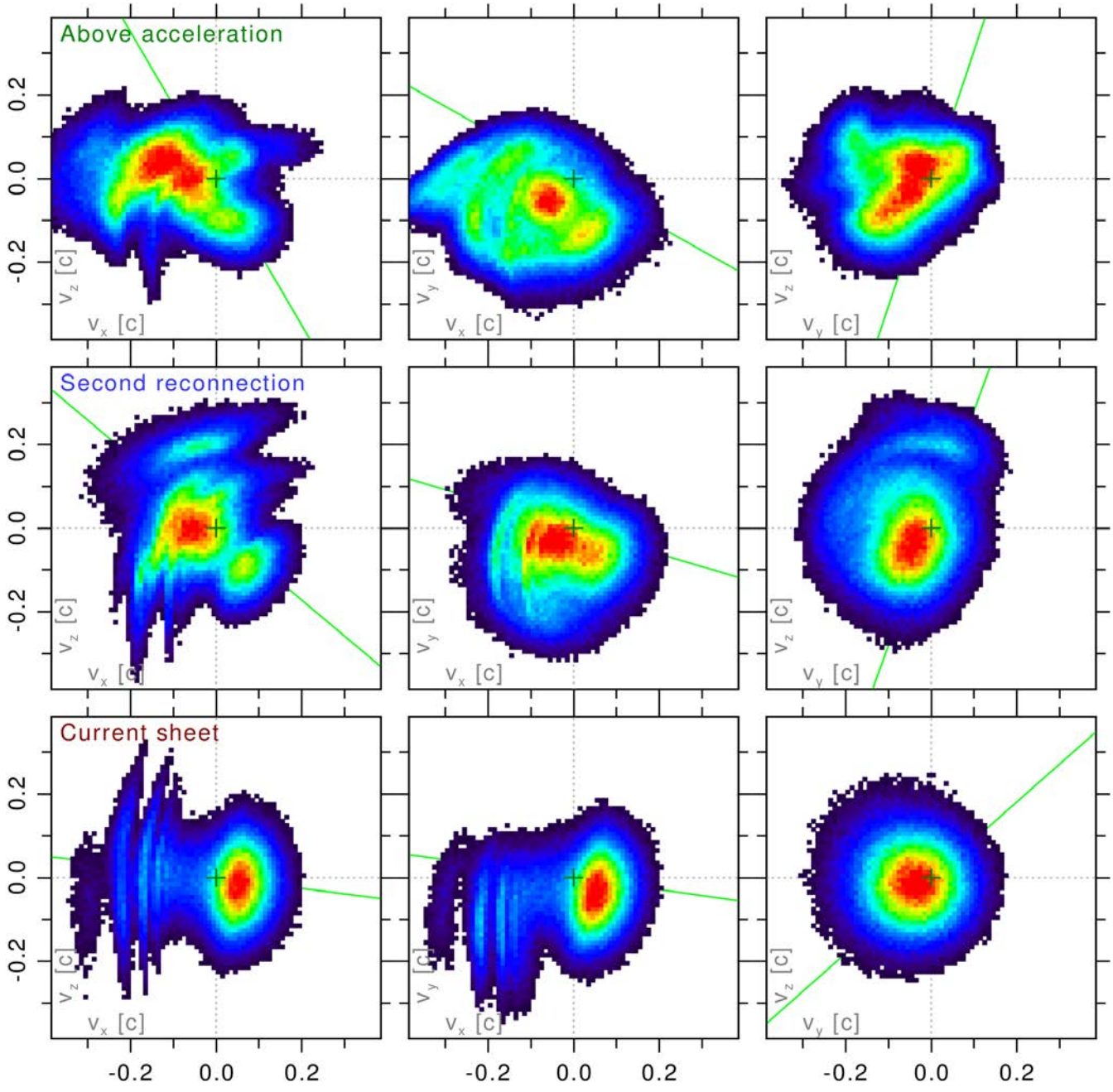

SOLAR SYSTEM

IWF is engaged in many missions, experiments and corresponding data analysis addressing solar system phenomena. The physics of the Sun and the solar wind, its interaction with solar system bodies, and various kinds of planetary atmosphere/surface interactions are under investigation.

SUN & SOLAR WIND

The Sun's electromagnetic radiation, magnetic activity, and the solar wind are strong drivers for various processes in the solar system.

SOLAR ORBITER

Solar Orbiter is a future ESA space mission to investigate the Sun, scheduled for launch in 2020 (Fig. 20). Flying a novel trajectory, with partial Sun-spacecraft corotation, the mission plans to investigate in-situ plasma properties of the near solar heliosphere and to observe the Sun's magnetized atmosphere and polar regions.

IWF builds the digital processing unit (DPU) for the *Radio and Plasma Waves (RPW)* instrument aboard *Solar Orbiter* and has calibrated the *RPW* antennas, using numerical analysis and anechoic chamber measurements. Furthermore, the institute contributes to the magnetometer.

RPW will measure the magnetic and electric fields at high time resolution and will determine the characteristics of magnetic and electrostatic waves in the solar wind from almost DC to 20 MHz. Besides the 5 m long antennas and the AC magnetic field sensors, the instrument consists of four analyzers: the thermal noise and high frequency receiver; the time domain sampler; the low frequency receiver; and the bias unit for the antennas. The control of all analyzers and the communication will be performed by the DPU, developed by IWF.

In 2017, the so called *Main Electronics Box (MEB)*, containing both DPUs, the power supply and the four analyzers, has been finally integrated under the leadership of LESIA (Laboratoire d'Etudes Spatiales et d'Instrumentation en Astrophysique) and CNES (Centre National d'Etudes Spatiales). The environmental tests have been successfully completed and the instrument has been delivered to ESA for further integration onto the spacecraft.

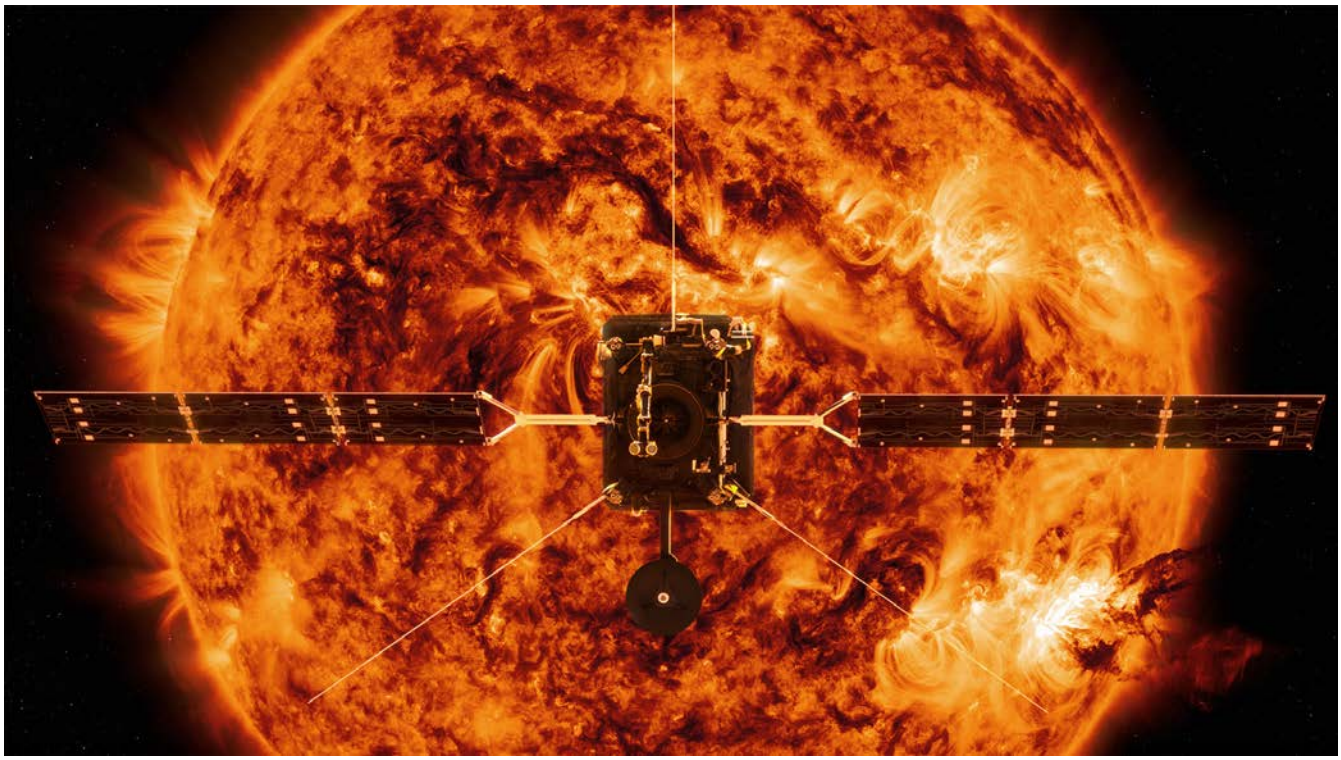

Fig. 20: Artist's impression of ESA's *Solar Orbiter* in front of the Sun [not to scale; Copyright: Spacecraft: ESA/ATG medialab; Sun: NASA/SDO/ P. Testa (CfA)].

SPACE WEATHER PREDICTION VERIFIED

Solar storms are formed by incredibly powerful explosions on the Sun and travel as clouds of plasma threaded by magnetic fields through the solar system. Depending on their propagation direction, they may impact planets such as Earth, where they elicit colorful aurorae or, in very seldom cases, can lead to power failures with potentially tremendous economical and societal effects, thus posing a serious natural hazard.

The solar storm impact can be forecasted when using a special type of instrument on the *STEREO* mission that can actually image the solar storms as they propagate toward the planets (see Fig. 20) and even as they sweep over them. The analysis included two thirds of a solar cycle with eight years of data, and spacecraft at Mercury, Venus, Earth, and in the solar wind to check on the correctness of our predictions. This includes data from the *Venus Express* magnetic field instrument, which was built at IWF.

Forecasts of the solar storm arrival time were possible to within about 2.5 hours, with a spread of +/- 16 hours, and for one correct impact there are two to three false alarms. These results show that accurate space weather forecasts with a mission at the Sun-Earth L5 point could be possible, although modeling accuracy should clearly be further improved. Data returned by the upcoming missions *Parker Solar Probe, Solar Orbiter* and *BepiColombo* are expected to lead to groundbreaking advances in this field.

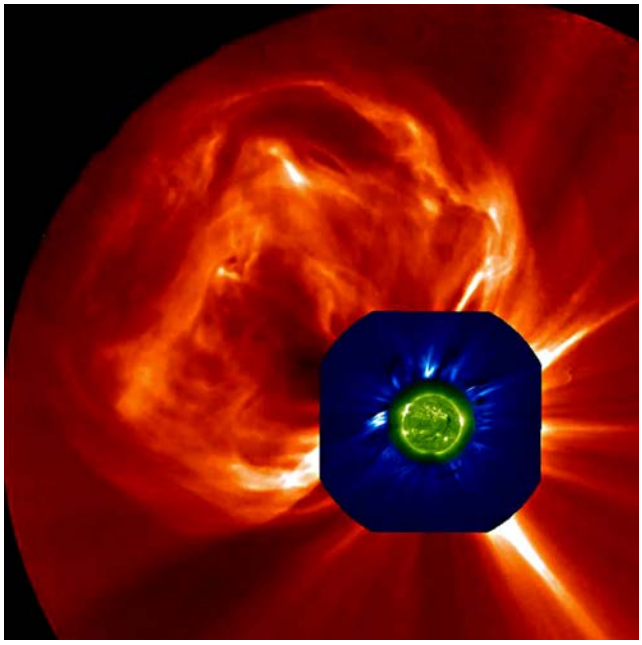

Fig. 20: A solar storm imaged by the *STEREO* mission (Copyright: NASA/ STEREO).

PLASMA BETA AT THE SUN

A crucial physical quantity in a star's atmosphere is the ratio between thermal and magnetic pressure, called plasma beta. With recent 3D simulation results, plasma beta could be estimated for the solar corona from a magneto-hydrodynamic model of a magnetically active region with some surrounding quiet Sun area.

The new data show that the possible value range for beta is orders of magnitude larger than previously thought if also more quiet regions are considered, which usually cover about 98% of the Sun's surface. In particular, beta may become larger than unity in the whole corona, which is a surprise for magnetic field modeling.

With this fact in mind, a new mechanism for the formation of a penumbra, the gray surroundings of a dark sunspot, could be formulated. The chromosphere surrounding the sunspot is connected to the corona and gets loaded with cooling material. Due to a beta larger than unity, field lines can be dragged down to the surface, where a horizontal magnetic field allows for the characteristic features of a forming penumbra, like the counter-Evershed flows (see green arrow in Fig. 21), horizontal magnetic field, and hence strongly elongated granules. These features have been observed but had not yet been understood.

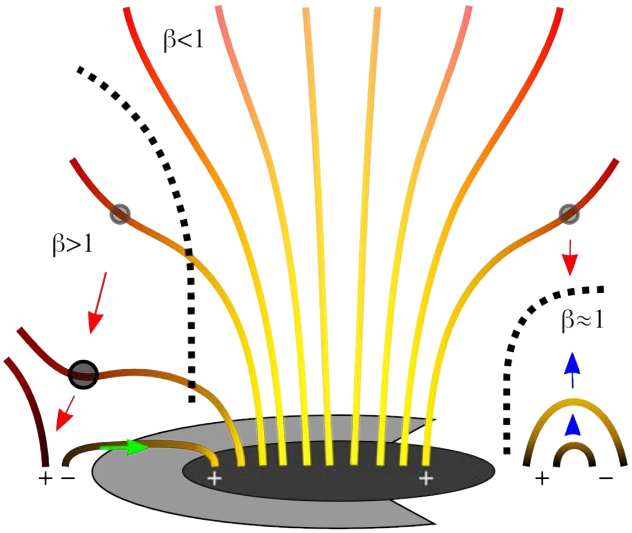

Fig. 21: Field lines above and around the sunspot (black). Cooling material may drag down the field because plasma beta may well be larger than unity (red arrows). This allows for the formation of the penumbra (gray). Emerging flux hinders the formation of the penumbra (blue arrows).

MERCURY

Mercury is now in the center of attention because of the upcoming ESA/JAXA *BepiColombo* mission. The planet has a weak intrinsic magnetic field and a mini-magnetosphere, which strongly interacts with the solar wind.

BEPICOLOMBO

Two spacecraft will simultaneously explore Mercury and its environment: the Japanese *Magnetospheric (MMO)* and ESA's *Planetary Orbiter (MPO)*. IWF plays a major role in developing the magnetometers for this mission: it is leading the magnetometer investigation aboard the *MMO (MERMAG-M)* and is responsible for the overall technical management of the *MPO* magnetometer *(MERMAG-P)*. For *MPO*, IWF also leads the development of the *Planetary Ion CAMera (PICAM*), an ion mass spectrometer with imaging capability, which is part of the *SERENA* instrument suite, to explore the composition, structure, and dynamics of the exo-/ionosphere. The launch on board of an Ariane 5 from Europe's spaceport in French Guiana is confirmed for October 2018.

The year 2017 saw the final environmental and detailed functional test campaigns for both spacecraft on ground including EMC testing on *MPO* level as well as acoustic and vibration testing in full flight configuration (see Fig. 22). Beside the support of these tests, the instrument teams at IWF participated in other system level testing, in particular in the validation of the autonomous on-board control procedures (OBCPs), which were checked in operational scenarios. In parallel, the procedures for the Near-Earth Commissioning Phase were brought to a mature status, and the detailed planning for the Venus flybys and cruise operations was started. The flight software and the data processing are continuously improved. The *MPO* units, *MERMAG-P* and *PICAM*, passed their Instrument Flight Acceptance Reviews, so they were formally permitted for the journey to Mercury.

Fig. 22: Examining the *BepiColombo* stack in ESA's test center. The people give a sense of the scale of the full spacecraft stack, which is more than 6 m high (Copyright: ESA–C. Carreau, CC BY-SA 3.0 IGO).

ROTATIONAL HISTORY OF MERCURY

The rotation of Mercury is strongly coupled to its orbital motion around the Sun: while one year on Mercury approximately lasts about 88 days, one mercurial day is very close to 2/3 of this value. Mercury, very probably, was not always situated in this current 3:2 spin-orbit resonance. Planet formation studies usually assume that planets form at much higher rotation rates. Over time dissipative effects like tidal friction slow down the rotation to allow temporary coupling between the orbit and the spin periods. The process stops when the 1:1 spin-orbit resonance is reached, i.e. if the lengths of the planetary "days" and "years" coincide.

While the phenomenon of the coupling between the spin and orbit periods of celestial bodies is well understood, the consequence of the internal gravity field and the coupling on the orientation of their rotation axes in space requires further investigations. The strong influence of the presence of a p:q spin-orbit resonance on its spin axis was shown (Fig. 23), and present physical theories were extended to include this effect. The *BepiColombo* mission will allow to scrutinize scientific theories about the origin and evolution of planet Mercury including its orbital and rotational history. A large amount of extra-solar planets are found very close to their host star. Subsequently, the same physics related to the spin-orbit coupling applies, and Mercury therefore serves as the best candidate to test new scientific findings before applying them to more distant objects that cannot be reached by space missions in the near future.

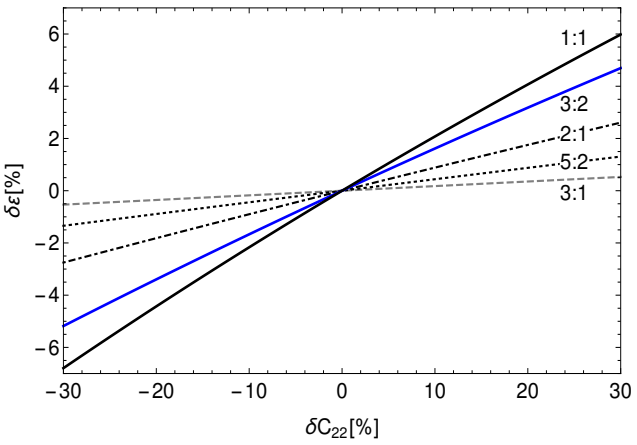

Fig. 23: Variations of the orientation of the spin-axis (ordinate) versus equatorial mass asymmetry (abscissa) for different p:q spin-orbit resonances.

VENUS & MARS

Two terrestrial planets are located just inside, Venus at 0.7 AU, and outside, Mars at 1.5 AU, the Earth's orbit around the Sun. Venus has a radius slightly smaller than Earth and is differentiated, but does not exhibit an internal magnetic field. Mars has half the radius of the Earth, is also differentiated, but only exhibits remnant surface magnetization of a now defunct internal dynamo. Venus is characterized by a very dense, Mars by a very tenuous atmosphere. Both planets generate a so-called induced magnetosphere by their interaction with the solar wind.

INSIGHT

NASA's Mars mission *InSight* will launch in May 2018. IWF is participating in *HP³ (Heat flow and Physical Properties Probe)*, which consists of a cylindrical body with a built-in hammering mechanism to drive the probe at least 3 m into the ground. It will measure the interior heat flux of Mars as well as the thermal and mechanical properties of the Martian soil. In order to describe and predict the penetration performance of *HP³*, two numerical tools were developed and tested at IWF: a pile driving model able to predict the overall behavior of the mole during penetration and a numerical model (Fig. 24), allowing to predict the response of the granular medium surrounding the mole and its stress behavior. These models have been validated by comparison with soil-mechanical tests in the lab.

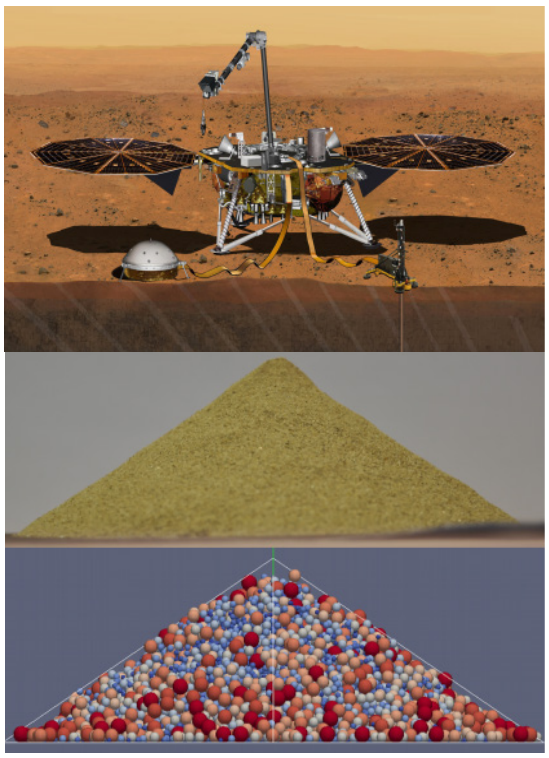

Fig. 24: *InSight* spacecraft after landing on Mars with the main instruments in deployed configuration (top) and a comparison of a soil-mechanical lab test with the result of our numerical particle interaction code (bottom).

EXOMARS

Several mechanisms devoted to retrieval and transportation of drill cores have been tested under Mars environmental conditions at IWF, among them the milling-and-crushing as well as the dosing device responsible for feeding various soil analysis instruments aboard ESA's *ExoMars* rover. In particular, possible cementation of soil samples under the influence of condensing water vapor was investigated.

CHINESE MARS MISSION

China plans a Mars orbiter, lander, and rover mission to be launched in 2020. The main mission will conduct a comprehensive remote sensing of the Red Planet, as well as surface investigation. IWF will contribute to a magnetometer.

ESCAPE AND FRACTIONATION OF NOBLE GASES FROM EARLY VENUS

Different early evolution scenarios for Venus have been investigated and realistic cases, by comparing modeled noble gas isotope ratios with present observations in Venus' atmosphere, were used as constraints. Isotope ratios of $^{20}Ne/^{22}Ne$ and $^{36}Ar/^{38}Ar$ could be reproduced (see Fig. 25), starting from solar values, under hydrodynamic escape conditions. Solutions for different solar EUV histories were found, as well as assumptions about the initial atmosphere, either a pure steam atmosphere (i.e., H_2O, CO_2) or a mixture with accreted hydrogen (H_2-dominated) from the protoplanetary nebula. The results generally favor an early accretion scenario with a small amount of residual H_2 from the protoplanetary nebula and a low-activity Sun, because in other cases too much CO_2 is lost during evolution, which is inconsistent with Venus' present atmosphere. Important issues are likely the time at which the initial steam atmosphere is outgassed and/or the amount of CO_2 which may still be delivered at later evolutionary stages. A late accretion scenario can only reproduce present isotope ratios for a highly active young Sun, but then unrealistically massive steam atmospheres (few kbar) would be required.

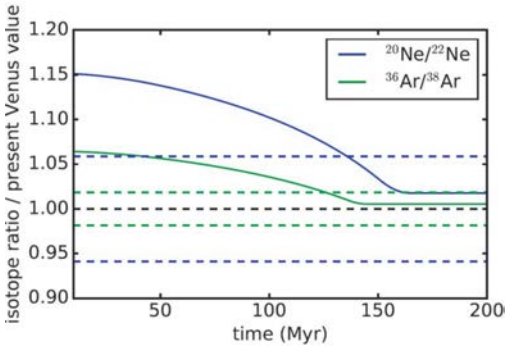

Fig. 25: Model results for a weakly active young Sun (slow rotator) of a case in which the atmospheric $^{20}Ne/^{22}Ne$ and $^{36}Ar/^{38}Ar$ isotope ratios of Venus can be reproduced after about 150 Myr of evolution from initially solar ratios. The dashed lines show the uncertainties of the present measurements (black line) in Venus' atmosphere.

ASYMMETRIES IN THE MAGNETOSHEATH FIELD DRAPING ON VENUS' NIGHTSIDE

Draping features of the interplanetary magnetic field around nonmagnetic bodies have been studied in detail in numerical simulations and also from observations. Existing analytical and numerical work show a kink in the draped field lines in the near magnetosheath on the quasi-parallel side of the bow shock.

Data from the *Venus Express* mission (2006–2014) are analyzed for differences in the draping pattern between the quasi-parallel and quasi-perpendicular side of the bow shock. From these magnetometer data, the kink in the field lines occurring only on the quasi-parallel side is clearly identified from the change of sign in the field component parallel to the solar wind velocity, as shown in Fig. 26.

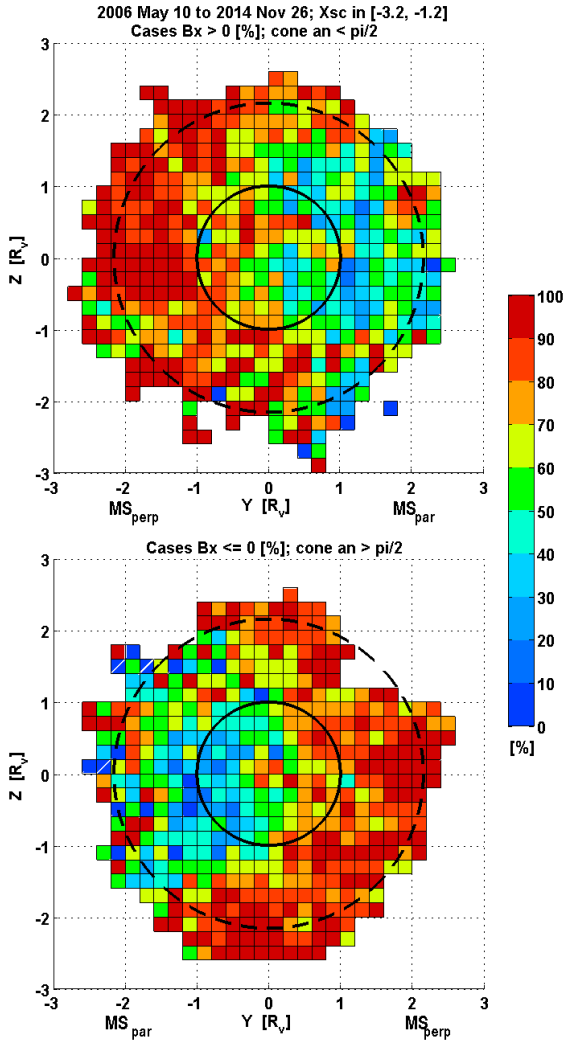

Fig. 26: Cases per bin with change in sign of Bx, in % of observed cases, Xsc in [-3.2, -1.2]. Representation as seen from the Sun, in VBE reference frame. The solid circle indicates Venus, the dashed circle the model bow shock at terminator. Top: For inward IMF, $\theta < 90°$ and BxSW > 0; the initially positive BxSW value is changed to negative values on the right-hand side of the MS, which here is MS_{par}. Bottom: For outward IMF, $\theta > 90°$ and BxSW < 0; the initially negative BxSW value changes to positive values on the left-hand side, which here is MS_{par}.

ATMOSPHERIC ESCAPE FROM MARS

With a Monte Carlo model the escape of energetic (hot) O and C atoms from the Martian atmosphere was investigated during its history corresponding to 1, 3, 10, and 20 times the present solar EUV flux. The increase of the production rates due to higher number densities resulting from the higher EUV flux competes against the expansion of the thermosphere and corresponding increase in collisions. The escape due to photodissociation increases with increasing EUV levels. For the escape via some other reactions, e.g., dissociative recombination of O_2^+, this is only true until the EUV level reaches 10 times the present EUV flux and then the rates start to decrease.

Furthermore, the results show that Mars could not have had a dense atmosphere at the end of the Noachian epoch (see Fig. 27), since such an atmosphere would not have been able to escape until today. In the pre-Noachian era, most of the magma ocean and volcanic activity-related outgassed CO_2 atmosphere could have been lost thermally until about 4 Gyr ago, when nonthermal loss processes such as suprathermal atom escape became dominant.

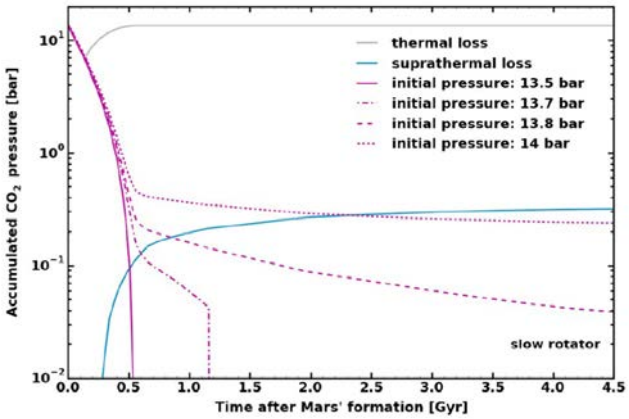

Fig. 27: Catastrophic outgassing of an initial steam atmosphere, related to a magma ocean, may have occurred after proto-Mars finished its formation within the first 10 Myr after the origin of the Sun. The surface pressure evolution resulting from thermal and hot (i.e., C, O) CO_2 escape of an initially outgassed CO_2 atmosphere between 13 and 14 bar are shown, if the young Sun was assumed to be a slow rotator. In the beginning of Mars's atmospheric evolution, thermal escape is much higher than hot atom loss. Only initial CO_2 atmospheres with surface pressures <14 bar, most likely reproduce the present CO_2 surface pressure level of about 7 mbar, if one assumes that the subsurface contains only negligible amounts of carbonates.

JUPITER & SATURN

Jupiter and Saturn, the two largest planets in our solar system, mainly consist of hydrogen and helium. They also have layers in their atmospheres with clouds consisting of ammonia, ammonium hydrosulfide and water, in which weather phenomena occur. Both planets are magnetized and rotate rapidly, leading to rotationally dominated magnetospheres, where strong sources of radio emissions are located.

JUNO

The main scientific goal of NASA's *Juno* spacecraft, launched in 2011, is to measure Jupiter's composition, gravity, and magnetic field, and to investigate its polar magnetosphere. IWF has calibrated the antenna system of the *Juno Waves* instrument.

JUICE

ESA's first Large-class mission *JUpiter ICy moons Explorer (JUICE)* is planned to be launched in 2022 and to arrive at Jupiter in 2030. *JUICE* will spend at least three years making detailed observations of the gas giant Jupiter and three of its largest moons, Ganymede, Callisto, and Europa. IWF is taking part as Co-I for three different selected instrument packages.

The *Jupiter MAGnetometer (J-MAG)* is led by Imperial College London and will measure the magnetic field vector and magnitude in the bandwidth DC to 64 Hz in the spacecraft vicinity. It is a conventional dual sensor fluxgate configuration combined with an absolute scalar sensor based on more recently developed technology. Science outcome from *J-MAG* will contribute to a much better understanding of the formation of the Galilean satellites, an improved characterization of their oceans and interiors, and will provide deep insight into the behavior of rapidly rotating magnetized bodies. IWF supplies the atomic scalar sensor for *J-MAG*, which is developed in collaboration with TU Graz. In 2017, the Engineering Model was developed and the Critical Design Review was passed.

The *Particle Environment Package (PEP)* is a plasma package with sensors to characterize the plasma environment of the Jovian system and the composition of the exospheres of Callisto, Ganymede and Europa. IWF participates in the *PEP* consortium on Co-I basis in the scientific studies related to the plasma interaction and exosphere formation of the Jovian satellites.

Finally, IWF is responsible for the antenna calibration of the *Radio and Plasma Wave Investigation (RPWI)* instrument. In 2017, a genetic algorithm was used in numerical simulations to find the antenna orientation with the best reception properties. As a result, the orientation of the radio antenna triad (three orthogonal antennas on the magnetometer boom) has now been fixed.

CASSINI

In 2017, the *Cassini* mission was in its final year. From November 2016 until April 2017 the spacecraft made ring-grazing orbits with periapsis passes close to the F-ring and apoapsis passes around Titan's orbit. A slight gravitational nudge by Titan on 22 April (last close Titan flyby) was used to change the periapsis to the unexplored region between Saturn's upper atmosphere and its innermost D-ring. *Cassini* performed 22 of these so-called proximal orbits during the following five months. Finally, on 15 September the spacecraft entered Saturn's atmosphere (see Fig. 28) and burned up and disintegrated like a meteor.

During its 20 years in space (7 year cruise plus 13 years in 294 orbits around Saturn) *Cassini* has delivered 635 GB of science data, which to date have been investigated in almost 4000 scientific publications. More than 50 of them include scientists from IWF which participated in the team of the *Cassini Radio and Plasma Wave Science (RPWS)* instrument.

Fig. 28: This artist's concept shows an over-the-shoulder view of *Cassini* making one of its Grand Finale dives over Saturn (Credit: NASA/JPL-Caltech).

LIGHTNING ACTIVITY ON SATURN

The radio emissions from lightning have been monitored by the *Cassini RPWS* instrument from 2004 until 2017. Fig. 29 shows that Saturn lightning storms can last from a few days up to several months and that there were also long time intervals with no lightning activity. The latter was the case for the last four years of the mission, and the absence of lightning storms after October 2013 could be explained by a kind of convective inhibition state of the atmosphere after the large thunderstorm of 2010/2011, which was called the Great White Spot (GWS).

Besides sferics at high frequencies in the MHz-range, lightning is known to emit whistler waves at very low frequencies which propagate along magnetic field lines from the source to the observer. The scarcity of whistler observations by *Cassini* (only one reported event in the literature) can be explained by *Cassini's* trajectory, since the stormy regions at latitudes around 35° North and South are connected to low magnetic L-shells which were traversed by *Cassini* only during orbit insertion and the proximal orbits of 2017. However, an intense search for lightning whistlers led to the detection of only three tentative events during the proximal orbits. This is probably due to the absence of lightning storms in 2017 as shown in Fig. 29.

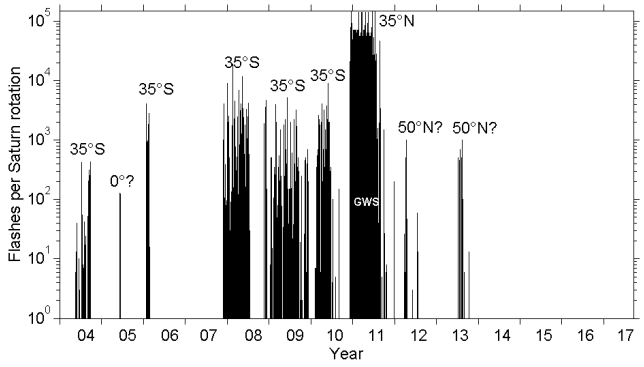

Fig. 29: Lightning flash rate measured by *Cassini RPWS* as a function of time (years from 2004 to 2017). The latitudes of the thunderstorms on Saturn are also denoted in the figure.

RADIO PROPAGATION: JUPITER VS. HOT JUPITERS

A study of the plasma conditions in the atmospheres of the Hot Jupiters HD 209458b and HD 189733b and for an HD 209458b-like planet at orbits between 0.2-1 AU around Sun-like stars was performed. It was found that the environmental conditions are such that the cyclotron maser instability (CMI), the process responsible for the generation of radio waves at Jupiter, most likely will not operate at hot Jupiters.

Hydrodynamically expanding atmospheres possess extended ionospheres, which fill-up the whole magnetosphere. This makes the magnetospheric plasma density so large that the plasma frequency is much higher than the cyclotron frequency (see Fig. 30). This prohibits the production of radio emission through CMI and also prevents the escape of radio waves. The structure of the upper atmosphere of gas giants around stars similar to the Sun changes between 0.2 and 0.5 AU from the hydrodynamic to a hydrostatic regime. This results in conditions similar to Jupiter, with a region of depleted plasma between the exobase and the magnetopause where the plasma frequency can be lower than the cyclotron frequency. In such an environment, highly energetic electrons, accelerated along the field lines towards the planet, can produce radio emission. However, even if the CMI could operate the extended ionospheres of Hot Jupiters are too dense to let the radio emission escape from the planets.

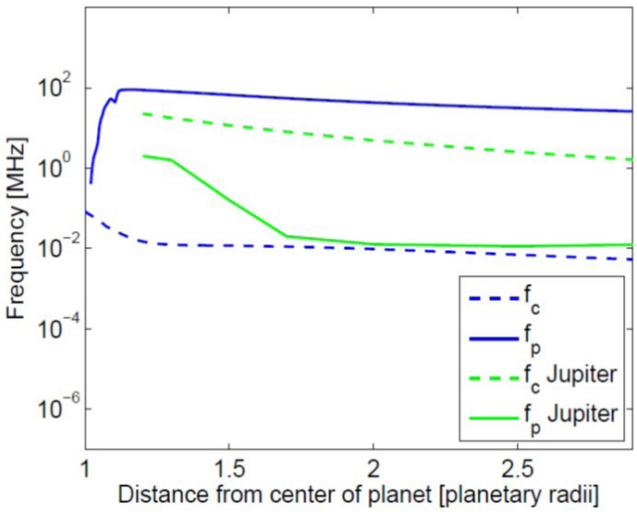

Fig. 30: Plasma frequency (solid blue line) and cyclotron frequency (dashed blue line) for HD 209458b for an equatorial surface magnetic field of 10^{-5} T as function of distance starting from the planetary transit radius along the equator. Solid and dashed green lines show the plasma and cyclotron frequency for Jupiter.

COMETS & DUST

Comets and interplanetary dust are the remainders of the building blocks of the solar system, although dust can also be created by collisions of e.g. asteroids. *Rosetta's* successful mission at comet 67P/Churyumov-Gerasimenko (67P/CG) gave new life to the study of comets and is the starting point for new future missions to asteroids and comets.

ROSETTA

The outstandingly successful *Rosetta* mission carried out the most sophisticated investigation of a comet to date. Between August 2014 and September 2016, eleven instruments analyzed comet 67P/CG, five of which with participation of IWF. The institute was Co-I for the *Rosetta Plasma Consortium (RPC)*, the *Rosetta Lander Magnetometer and Plasma Monitor (ROMAP)*, the *Multi-Purpose Sensor (MUPUS)*, and the *Cometary Secondary Ion Mass Spectrometer (COSIMA)*. Furthermore, IWF held the PI-ship for the *Micro-Imaging Dust Analysis System (MIDAS)*, an especially developed prototype instrument dedicated to the first ever analysis of most pristine cometary dust at the micro- to nanometer scale.

MIDAS was the first spaceborne atomic force microscope (AFM) and the only one to collect, handle and analyze cometary dust particles. Their shapes and spread on the targets indicate different degrees of alteration on collection that are similar to those found by *Rosetta's* other dust analysis instruments. The collected particles were investigated by AFM, i.e. sampling their surfaces with a very sharp tip. The main outcome is the 3D topography that allows to access the surface structure of nearly pristine cometary dust. *MIDAS* data revealed that cometary dust particles at the nm to µm scale are all hierarchical agglomerates, independent of size or collection time. Larger, about 10 µm sized particles disintegrate into their next smaller constituents upon investigation, which is a proof of their agglomerate nature and a sign for higher particle strengths at smaller scales. Detailed analyses of subunit strength and sizes are currently ongoing. Pristine structural diversity of cometary dust is found in the arrangement of the agglomerates: Whilst most of them are composed of subunits packed densely enough to prevent transparency (Fig. 31), a minority shows a low packing density that can be characterized by a fractal dimension of <2. The survival of those fragile particles has strong implications for the cometary formation and evolution.

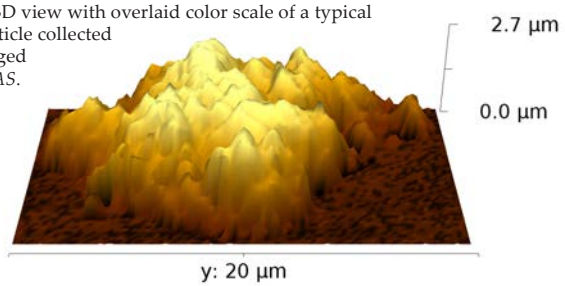

Fig. 31: 3D view with overlaid color scale of a typical dust particle collected and imaged by *MIDAS*.

CURRENT SHEETS IN 67P/CG'S COMA

The *Rosetta Plasma Consortium (RPC)* data were used to investigate the presence of current sheets in the coma of comet 67P/CG. The interaction of the interplanetary magnetic field (IMF) transported by the solar wind toward the outgassing comet consists amongst others of mass loading and field line draping near the nucleus. The draped field lines lead to so-called nested draping because of the constantly changing direction of the IMF.

It is shown that the draping pattern is strongly variable over the period of one month. Nested draping results in neighboring regions with oppositely directed magnetic fields, which are separated by current sheets. There are strong rotations of the magnetic field (Fig. 32) with associated current sheets that have strengths from several tens up to hundreds of nA/m². Only for June 2015 (panel C) do the data show "classical" large scale, nested draping. For May (A) and July (B) the changes in field direction happen about every hour (inset Bb).

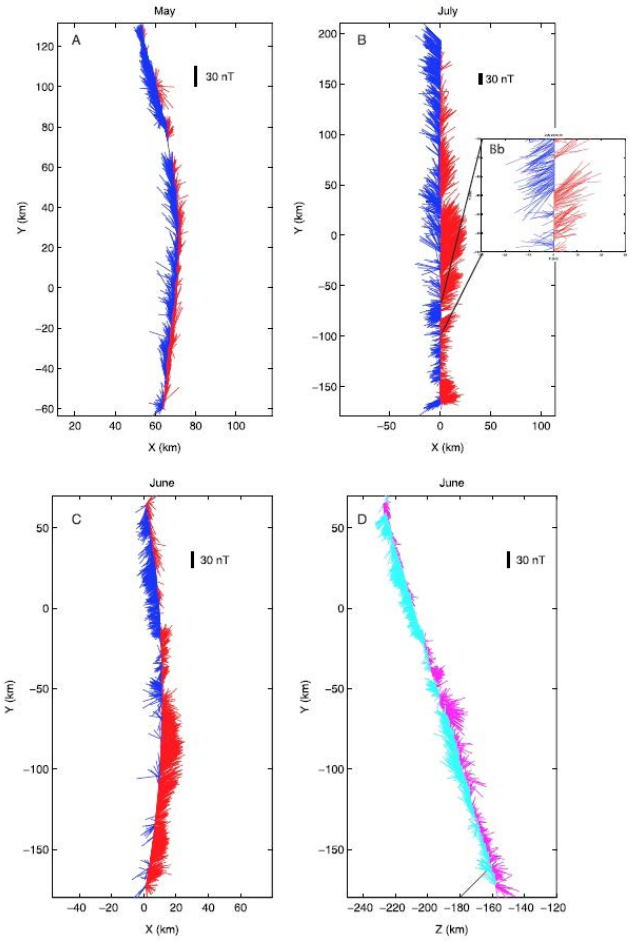

Fig. 32: Hedgehog plots of the magnetic field for three subsequent flybys. The XY plane for 1–8 May (A) and 24–31 July 2015 (B). The XY (C) and YZ (D) plane for 2–9 June. For (A), (B), and (C) the blue vectors show anti-sunward pointing magnetic field and the red vectors show sunward pointing magnetic field. For (D) the cyan vectors show downward pointing magnetic field and the magenta vectors show upward pointing magnetic field.

EXOPLANETARY SYSTEMS

The field of exoplanet research (i.e. investigation of planets orbiting stars other than the Sun) has developed strongly, in the past decade. Since the discovery of 51 Peg b, the first detected exoplanet orbiting a Sun-like star, about 3700 exoplanets, most of which in planetary systems, are now known. Improved instrumentation and analysis techniques have led to the finding of smaller and lighter planets, down to Earth-size, Earth-mass planets, some of which orbiting in the habitable zone of the cooler stars. However, super-Earths are now prime targets for atmospheric characterization, mostly because of their larger radii, which indicate the presence of a volatile-rich atmosphere and facilitate observations and analyses.

The two main exoplanet missions in which IWF is involved are *CHEOPS* and *PLATO*. The former will precisely measure the radii of already known planets to greatly improve their inferred density and hence provide a first characterization. The latter will instead look for planets in large portions of the sky, with the primary aim to find Earth-like planets in the habitable zone of Sun-like stars.

IWF concentrates on the study and characterization of planetary atmospheres using both theory and observations, focusing particularly on the analysis of exoplanet atmospheric escape and mass loss processes. Further research is conducted to study star-planet interactions and carry out atmospheric characterization through the collection and analysis of ground- and space-based observations.

CHEOPS

CHEOPS (CHaracterising ExOPlanet Satellite), to be launched in 2018, will study extrasolar planets and observe planetary systems at an unprecedented photometric precision. The main science goals are to find transits of small planets, known to exist from radial-velocity surveys, measure precise radii for a large sample of planets to study the nature of Neptune- to Earth-sized planets, and obtain precise observations of transiting giant planets to study their atmospheric properties. IWF is responsible for the *Back-End-Electronics (BEE)*, one of the two on-board computers, which controls the data flow and the thermal stability of the telescope structure.

In 2017, the Flight Model was manufactured and assembled. In cooperation with RUAG Space Austria and the test center at ESTEC the environmental tests at *BEE* level were completed successfully. Finally the unit was delivered to Bern for the mechanical and electrical integration with the *CHEOPS* optical system (Fig. 33).

Fig. 33: The *CHEOPS* team at the University of Bern assembles the instrument flight model in the clean room (Copyright: PlanetS).

PLATO

PLATO (PLAnetary Transits and Oscillations of stars) is ESA's third Medium-class mission, led by DLR. Its objective is to find and study a large number of extrasolar planetary systems, with emphasis on the properties of terrestrial planets in the habitable zone around solar-like stars. *PLATO* has also been designed to investigate seismic activity in stars, enabling the precise characterization of the host star, including its age. IWF contributes to the development of the *Instrument Controller Unit (ICU)* with the development of the *Router and Data Compression Unit (RDCU)*. Launch is expected in 2026.

PLATO consists of 24 telescopes for nominal and two telescopes for fast observations. Each telescope has its dedicated front-end-electronics, reading and digitizing the CCD content. Six nominal and two fast DPUs collect the data from the front-end-electronics and extract the areas of interest. The *RDCU* is a key element in the data processing chain, providing the communication between the DPUs and the *ICU*. The second task of the *RDCU* is the lossless compression of the science data. For performance reasons, the compression algorithm is implemented in an FPGA.

Main tasks in 2017 were the development of the *RDCU* prototype and the design of the VHDL code for the FPGA. The electronics design and the layout for the prototype was completed and the PCBs were ordered. The FPGA design concentrates on a core for the SpaceWire standard supporting both protocols packet mode and so called RMAP (remote memory access protocol) up to 100 Mbps data rate. These designs were completed and validated.

CUTE

CUTE (Colorado Ultraviolet Transit Experiment) is a NASA-funded 6U-form CubeSat to be launched in the first half of 2020 (Fig. 34). It will perform low-resolution transmission spectroscopy of transiting extrasolar planets at near-ultraviolet wavelengths. *CUTE* will study the upper atmospheres of short period extrasolar planets. The aim is to constrain atmospheric escape processes, which are key to understanding planetary evolution, and to detect heavy metals, which inform on the strengths of the atmospheric vertical velocities. Furthermore, *CUTE's* continuous temporal coverage of planetary transits will allow to detect transit asymmetries, which are possibly connected with the presence of planetary magnetic fields.

IWF is the only technological contributor to the mission outside of the University of Colorado (Boulder), where *CUTE* is being developed. IWF has started the development of the *CUTE* data simulator, following a detailed analysis of the optical system and tolerances, which has been completed.

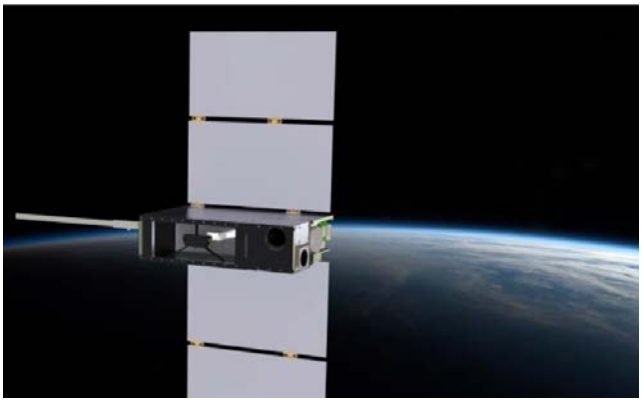

Fig. 34: Artist's impression of *CUTE* above the Earth (Credit: University of Colorado, Boulder).

OTHER TELESCOPES

Members of the institute obtained 20 orbits with the *STIS* spectrograph of the *Hubble Space Telescope (HST)* to perform far- and near-ultraviolet transmission spectroscopy of the HD3167c mini-Neptune (5 *HST* orbits) and HD189733b hot-Jupiter (15 *HST* orbits), respectively. Further eight nights of observations were obtained with the *FORS2* instrument at the *Very Large Telescope (VLT)* at the Paranal site of the European Southern Observatory (ESO), in Chile. The majority of these spectroscopic observations, conducted during planetary transits, will be used to study the physical properties of the atmosphere of five close-in giant planets. A small part of the observations will be used to derive the orbital properties of a binary system composed of a late-type star and a neutron star, where the latter is the remnant of an historical Ca-rich supernova.

OVERABUNDANCE OF LOW-DENSITY NEPTUNE-LIKE PLANETS

The last years have seen an increasing number of detections of close-in, low-density planets. The existence, formation, and evolution of such planets are difficult to understand: their atmospheres should be characterized by very strong escape. It has been shown that planets for which Λ (the value of the Jeans escape parameter calculated at the observed planetary radius and mass, for the planet's equilibrium temperature, and considering atomic hydrogen) is smaller than 15-35 lie in the "boil-off" regime. This means that they experience extremely strong Jeans escape, which is driven by the atmospheric thermal energy and low planetary gravity.

To date 167 close-in, Neptune-like planets, for which both planetary radius and mass (mostly from transit timing variations) have been measured, are known. Upper atmosphere modeling of these planets shows that 25 of them (about 15%) are simultaneously consistent with the presence of H-dominated atmospheres and extremely high escape rates (Fig. 35). This constitutes a contradiction, since the hydrogen envelopes cannot be retained given the high mass loss rates. Instead, either hydrodynamic models overestimate the mass loss rates, transit timing variation measurements underestimate the planetary masses, optical transit observations overestimate the planetary radii (e.g., high-altitude clouds), or Neptunes have consistently higher albedo than Jupiter planets.

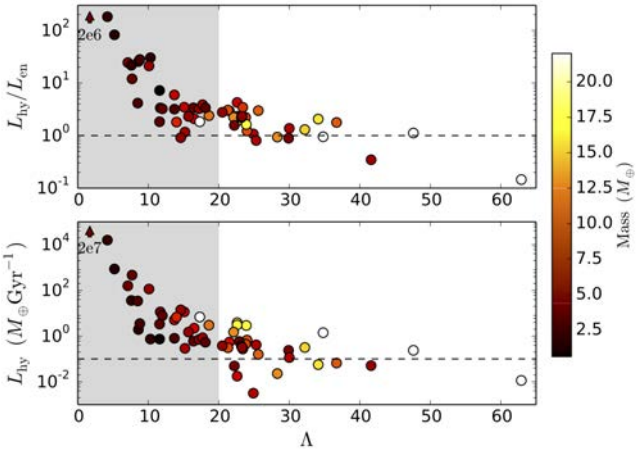

Fig. 35: Top: Ratio between the hydrodynamic and energy-limited mass loss rates vs. the Jeans escape parameter Λ. The color scale denotes the planetary mass. The gray area marks the region with dominant extreme thermal mass loss rate. The labeled triangle denotes the mass loss value for the extreme case of Kepler-33c. Bottom: Hydrodynamic mass loss rate vs. Λ.

ISM ABSORPTION EFFECT ON STELLAR ACTIVITY MEASUREMENTS

Past ultraviolet and optical observations of stars hosting close-in Jupiter-mass planets have shown that some of these stars present an anomalously low chromospheric activity level. For the planet host WASP-13, observations have indicated that the anomaly is caused by absorption from the intervening interstellar medium (ISM). Synthetic stellar photospheric spectra were combined with varying amounts of chromospheric emission and ISM absorption. The effect of ISM absorption on CaII line core activity measurements by varying several instrumental (spectral resolution), stellar (projected rotational velocity, effective temperature, and CaII chromospheric emission flux), and ISM parameters (relative velocity between stellar and ISM lines, broadening b-parameter, and CaII ISM column density) have been studied in detail.

For relative velocities between stellar and ISM lines smaller than 30-40 km/s and for ISM CaII column densities larger than 10^{12}, the ISM absorption has a significant influence on activity measurements (Fig. 36). Direct measurements and three dimensional maps of the Galactic ISM absorption indicate that an ISM CaII column density of 10^{12} is typically reached by a distance of 100 pc along most sight lines. In particular, for a Sun-like star lying at a distance of 100 pc, the bias in the measured activity parameter is expected to be of about the same size as the typical measurement uncertainties. Correcting for the ISM absorption bias may allow one to identify the origin of the anomaly in the activity measured for some planet-hosting stars.

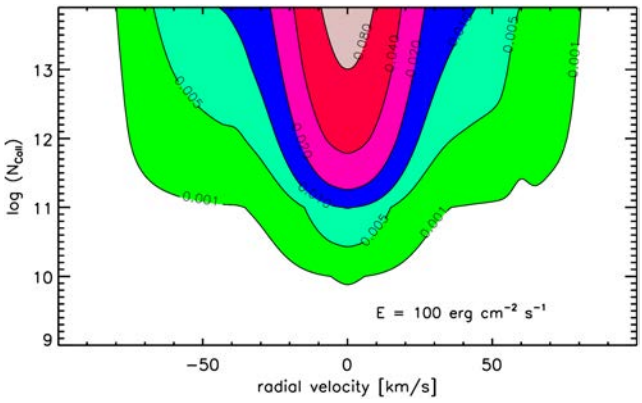

Fig. 36: Color-coded difference between the activity parameter measured without ISM absorption and that obtained after adding varying amounts of ISM absorption (y-axis) as a function of the relative velocity between stellar and ISM lines. The total applied CaII chromospheric emission is 100 erg cm^{-2} s^{-1}.

STRONG Na/K ABSORPTION IN THE WASP-103B TRANSMISSION SPECTRUM

Transmission spectroscopy has become a prominent tool for characterizing the atmospheric properties of close-in transiting extrasolar planets. It is sensitive to the absorption features imprinted by the planetary atmosphere on the stellar light that passes through it during transit. In this configuration the planetary day-night terminator region is probed. WASP-103b is one of the hottest (2500 K) and most massive (1.5 Jupiter masses) planets so far studied with transmission spectroscopy. Furthermore, the planet orbits its host star at a separation of less than 1.2 times the Roche limit and is predicted to be strongly tidally distorted.

Three transits of WASP-103b have been observed with the *GMOS-North* spectrograph installed at the *Gemini North* telescope in Hawaii to look for the signature of Na, K, and H_2O in the planetary atmosphere. The data were analyzed making use of the "common noise model" approach, which allows to significantly reduce systematic noise. The three individual transmission spectra agree well among each other and reveal the presence of strong absorption features of both Na and K (Fig. 37). The lack of a strong scattering slope suggests also the presence of either a clear atmosphere or of a cloud deck at pressures higher than 10 mbar, below the region probed by the observations. These observations corroborate tentative trends between cloud occurrence and planetary properties, in particular the absence of observable clouds for highly-irradiated planets.

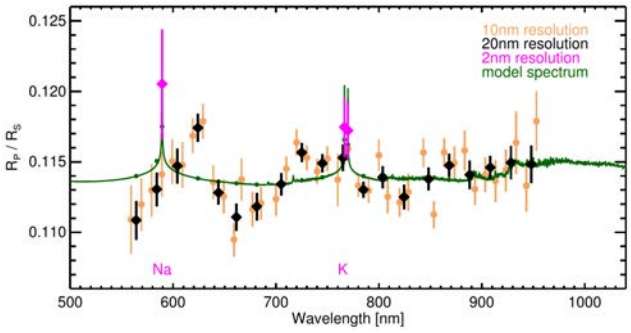

Fig. 37: Transmission spectrum of WASP-103b as observed with *GMOS-North*. Measurements obtained with 10 and 20 nm wide bins are shown as brown filled circles and black squares, respectively. Measurements in 2 nm wide bins centered on the Na feature as well as on both components of the K feature are shown in magenta. The best fitting model transmission spectrum is shown by the green line.

STELLAR ROTATION VARIABILITY AND STARSPOT DIAGNOSTICS

The evolution of starspot activity patterns is controlled by a hitherto unresolved mixture of drivers from near-subsurface small-scale plasma flows up to giant turbulence deep inside the star. Manifestations of the related mechanisms were separated using the difference in stability of the starspot distributions on global and hemispherical scales in 1998 main sequence stars observed by the *Kepler* mission. Two main mechanisms were revealed: 1) the diffusive decay of long-living spots in activity complexes of stars with saturated magnetic dynamos, and 2) the spot emergence, which is modulated by gigantic turbulent flow in the convection zones of stars with a weaker magnetism. Subdiffusion in stellar photospheres was also revealed from these observations for the first time. These results open a way for investigation of stellar surface flows as well as deep convection, which is yet inaccessible through asteroseismology. A diagnostic diagram was developed, that allows the differentiation and selection of stars for future studies of starspot phenomenology, magnetic diffusion and deep mixing.

INDUCTION HEATING & MAGMA OCEAN FORMATION ON TRAPPIST-1'S PLANETS

M-type stars often host detectable rocky planets. Seven small planets were discovered in the M star system TRAPPIST-1, which has an observed magnetic field of 600 G. Electromagnetic induction heating (IH) as an energy source inside these planets was proposed for the first time. If the stellar rotation and magnetic dipole axes are inclined to each other, IH can melt the upper mantle and increase volcanic activity, and develop magma oceans below the surface (Fig. 38). This process has important implications for habitability.

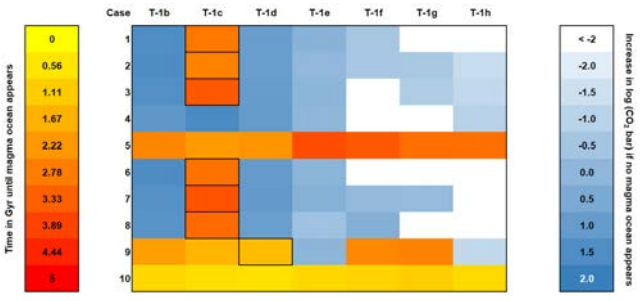

Fig. 38: Different parameters such as initial thermal boundary layer thickness, viscosity pre-factor, surface temperature, and initial mantle temperature are studied. The yellow–red color coding refers to the cases where a magma ocean appears. Thick lines indicate cases where a magma ocean forms when induction heating is considered, but is absent without. The blue color scale shows the log increase in total outgassed CO_2 in bar with respect to an evolution without induction heating after 5 Gyr of thermal evolution for cases in which no magma ocean appears.

LYMAN-ALPHA ABSORPTION AT TRANSITS OF HD209458B

To shed more light on the nature of the observed Ly-α absorption during transits of HD209458b and to quantify the major mechanisms responsible for the production of fast hydrogen atoms (so-called ENAs) around the planet, a 2D hydrodynamic multi-fluid modelling of the expanding planetary upper atmosphere has been performed, driven by the stellar XUV and its interaction with the stellar wind. The model self-consistently describes the escaping planetary wind and the generation of ENAs due to particle acceleration by radiation pressure and by charge-exchange between the stellar wind protons and planetary atoms.

The calculations in a wide range of stellar wind parameters and XUV flux values showed that under typical Sun-like star conditions the amount of generated ENAs is too small, and the observed absorption at the level of 6-8% can be attributed only to non-resonant natural line broadening. For lower XUV fluxes, e.g., during activity minima, the number of planetary atoms that survive photo-ionization and are the source of ENAs, increases resulting in up to 10-15% absorption at the blue wing of the Ly-α line, caused by the resonant thermal line broadening (Fig. 39). It has been found, that radiation pressure has a negligible contribution to the production of ENAs and the corresponding absorption.

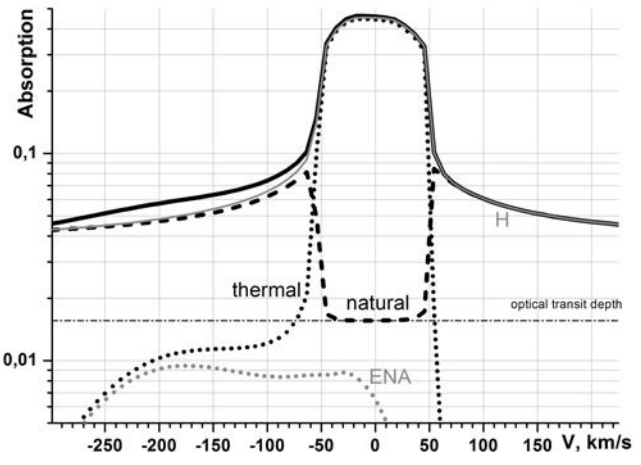

Fig. 39: The absorption profile of Ly-α line (thick solid line) under the typical conditions by HD209458b and slow stellar wind. A decomposition of the total absorption onto the resonant thermal (black dotted) and non-resonant natural line broadening (black dashed) parts is shown. Gray dotted and gray solid lines represent the contribution to the absorption of ENAs and planetary atomic hydrogen, respectively.

INFRASTRUCTURE

Instruments aboard spacecraft are exposed to harsh environments, e.g., vacuum, large temperature ranges, radiation, and high mechanical loads during launch. Furthermore, these instruments are expected to be highly reliable, providing full functionality over the entire mission time, which could last for more than a decade.

IWF owns several test facilities and special infrastructure for the production of flight hardware. A high-performance computer helps the scientists to cope with the enormous data, which have to be analyzed for space missions.

VACUUM CHAMBERS

The *Small Vacuum Chamber* is a manually controlled, cylindrical vacuum chamber (160 mm diameter, 300 mm length) for small electronic components or printed circuit boards. It features a turbo molecular pump and a rotary dry scroll forepump. A pressure level of 10^{-10} mbar can be achieved.

The *Medium Vacuum Chamber* has a cylindrical stainless steel body with the overall length of 850 mm and a diameter of 700 mm. A dry scroll forepump and a turbo molecular pump provide a pressure level of about 10^{-7} mbar. A target manipulator with two axes and an ion beam source are installed. This chamber mainly serves for functional tests of the ion mass spectrometer for *BepiColombo*.

The *Large Vacuum Chamber* has a horizontal cylindrical stainless steel body and door, a vision panel, two turbo molecular pumps and a dry scroll forepump. A pressure of 10^{-7} mbar can be achieved. The cylinder has a diameter of 650 mm and a length of 1650 mm. During shutdown the chamber is vented with nitrogen. A target manipulator inside the chamber allows for computer-controlled rotation of the target around three mutually independent perpendicular axes. The vacuum chamber is enclosed by a permalloy layer for magnetic shielding. To enable the baking of structures and components (to outgas volatile products and unwanted contaminations), the chamber is equipped with a heater around the circumference.

The *Thermal Vacuum Chamber* is fitted with two turbo molecular pumps, a dry scroll forepump, and an ion getter pump, which together achieve a pressure level of 10^{-6} mbar and allow quick change of components or devices to be tested. A thermal plate installed in the chamber and liquid nitrogen are used for thermal cycling in a temperature range between -90 °C and +140 °C. The vertically oriented cylindrical chamber allows a maximum experiment diameter of 410 mm and a maximum height of 320 mm.

The *Surface Laboratory Chamber* is dedicated to surface science research. It has a diameter of 400 mm and a height of 400 mm, extendable up to 1200 mm. One rotary vane pump and one turbo-molecular pump achieve a minimum pressure of 10^{-5} mbar. With an external thermostat the chamber temperature can optionally be controlled between -90 °C and +50 °C.

The *Sample Chamber* contains an 8µ particle filter and allows measurements of grain sample electrical permittivity. One rotary vane pump achieves a minimum pressure of 10^{-3} mbar.

HIGH-PERFORMANCE COMPUTER

Currently, the high-performance computing system LEO comprises 1320 CPU cores with a total of 8.25 TB of main memory (RAM), 72 TB of high-throughput SSD space for massive-parallel input/output, a storage server with about 300 TB raw capacity with different backup levels, one tape archive for long-time backup and storage, as well as an 54 Gbit/s Infiniband network switch connecting all main components with a nanosecond-latency network connection.

The LEO cluster completed its 10000th computing job, where each of these jobs requested a minimum of one compute node consisting of 40 CPU cores and 256 GB RAM. The range of applications available on the LEO cluster has recently been extended with ANSYS, a commercial software product used for structure mechanics, thermodynamics, fluid dynamics, and electro-magnetism.

OTHER TEST FACILITIES

The *Temperature Test Chamber* allows verifying the resistance of electronic components and circuits to most temperatures that occur under natural conditions, i.e., -40 °C to +180 °C. The chamber has a test space of 190 l and is equipped with a 32-bit control and communication system.

The second *Temperature Test Chamber* is used for fast cycling electronic components and circuit. The temperature range is -70 °C to +180 °C. The chamber has a test space of 37 l and is equipped with similar interfaces for communication.

The *Penetrometry Test Stand* is designed to measure mechanical soil properties, like bearing strength. The UV exposure facility is capable to produce radiation between 200-400 nm (UV-A, UV-B, UV-C).

MAGNETOMETER CALIBRATION

A three-layer magnetic shielding made from mu-metal is used for all basic magnetometer performance and calibration tests. The remaining DC field in the shielded volume is <10 nT and the remaining field noise is <2 pT/√Hz at 1 Hz. A special Helmholtz coil system allows generating field vectors of up to ±30000 nT around the sensor under test.

The *Magnetometer Temperature Test Facility* is used to test magnetic field sensors between -170 °C and +220 °C in a low field and low noise environment. Liquid nitrogen is the base substance for the regulation, which is accurate to ±0.1 °C. A magnetic field of up to ±100000 nT can be applied to the sensor during the test cycles.

FLIGHT HARDWARE PRODUCTION

Flight hardware is assembled and tested in the institute's *Clean Room* (Fig. 40), which is a class 10000 (according to U.S. Federal Standard 209e) certified laboratory with a total area of 30 m^2. It accommodates up to six engineers.

The laminar flow *Clean Bench* has its own filtered air supply. It provides product protection by ensuring that the work piece in the bench is exposed only to HEPA-filtered air (HEPA = High Efficiency Particulate Air). The internal dimensions are 118 x 60 x 56 cm^3.

The *Vapor Phase Soldering Machine* is suitable for mid size volume production. The maximum board size is 340 x 300 x 80 mm^3. Vapor phase soldering is currently the most flexible, simplest and most reliable method of soldering. It is ideally suited for all types of surface mounted device (SMD) components and base materials. It allows processing of all components without the need of any complicated calculations or having to maintain temperature profiles. For placing of fine pitch parts and rework of electronic boards an *Infrared Soldering Machine* with a precision placing system is used.

The *Fluid Dispensing System* DispenseMate 585 is a solder paste printer in a compact benchtop format. This machine allows a precise dosing of solder pastes on PCBs. As an option, a dispenser for precise glue application can be used. The range of motion is 525 x 525 mm.

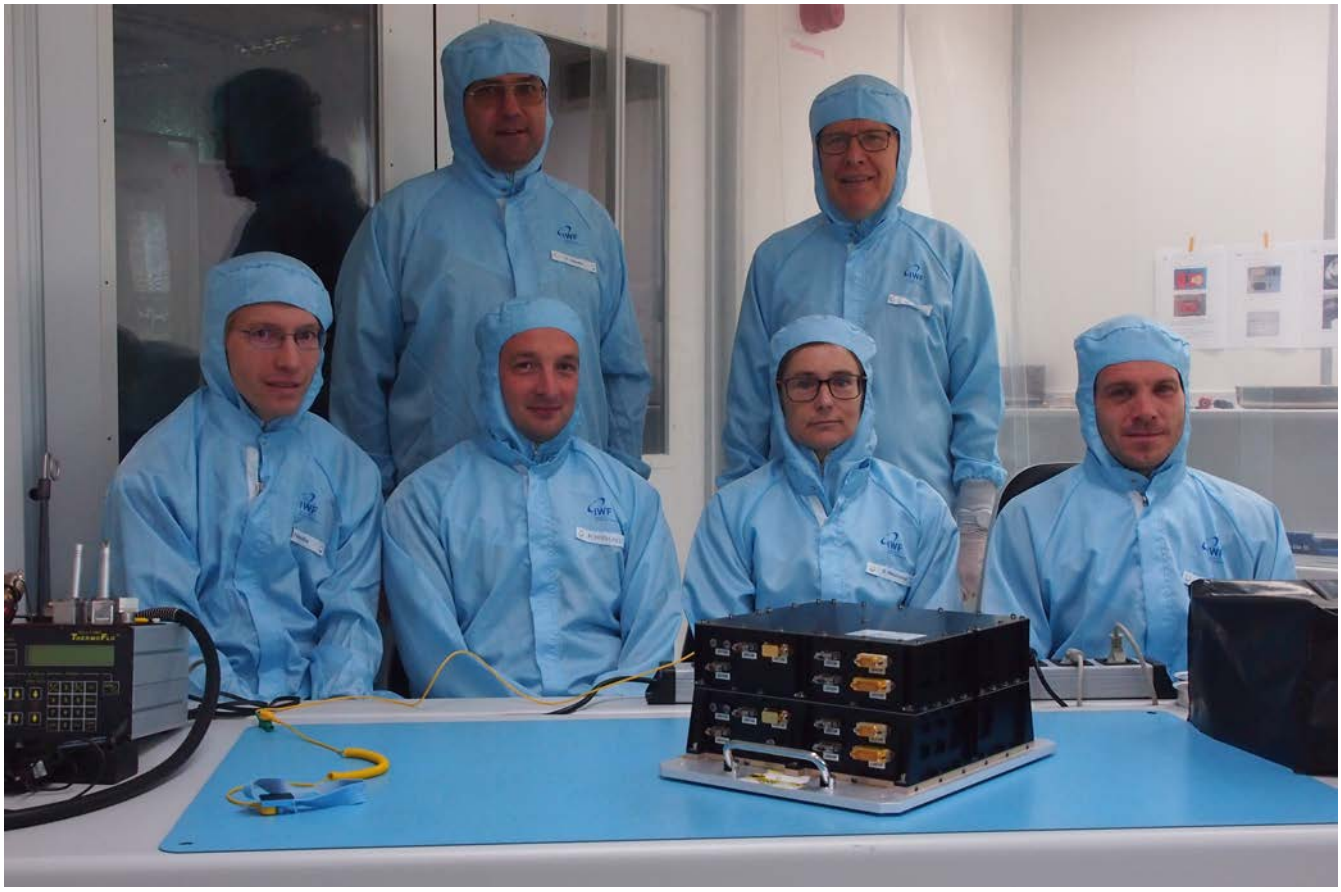

Fig. 40: *CHEOPS* hardware team with the flight model of the *Back-End-Electronics* in the institute's Clean Room.

OUTREACH

PUBLIC OUTREACH

IWF is actively engaged in science education and public outreach. In 2017, many different groups and school classes visited the institute and were guided through the labs and the planetary garden.

On 1 March, BMWFW invited IWF to take part in "YO!TECH - Lust auf Technik". More than 300 highschool students had the chance to learn about job profiles and educational possibilities in technology and natural sciences. Among the eleven exhibitors, IWF presented a functional model of the *CHEOPS* telescope.

On the same day, IWF director Wolfgang Baumjohann talked about "Managing Space" at FH OÖ Campus Steyr.

During summer time, seven high-school students performed an internship at IWF under the "Talente-Praktika" program of FFG. They worked on aurora, cometary surfaces and planetary materials, radio wave propagation, weather data, and VLF data analysis. In the framework of the "FEMtech" program of FFG, two young ladies from KFU Graz and TU Graz worked at IWF on meteorological time series and magnetospheric plasma physics.

On the occasion of *Cassini's* Grand Finale on 15 September, Bruno Besser gave a talk at Sternwarte Klagenfurt.

IWF opened its doors on 29 September in honor of the Austrian Astronomy Days, offering a series of six lectures and a dedicated children's program (Fig. 41).

Fig. 41: Children answering questions about our solar system during the Austrian Astronomy Days at IWF.

On 9 October, ESA, IWF, and others celebrated 30 years of Austrian membership in Graz (Fig. 42). IWF director Baumjohann participated in the round table "Space4Industry" and the institute presented its contributions to the *BepiColombo* mission.

Fig. 42: IWF members at "30 Jahre ESA-Österreich - Eine Erfolgsgeschichte".

IWF is partner in the "FFG-Talente-Regional" project "Freiflug - Die Geheimnisse des Fliegens". Its core is a travelling exhibition on aerospace for children and young adults, which was "launched" on 25 October at FH Joanneum in Graz.

AWARDS & RECOGNITION

In September, IWF director Baumjohann was elected as a member of „Academia Europaea" and IWF group leader Rumi Nakamura into the „Board of Trustees" of the „International Academy of Astronautics".

MEETINGS

Since more than 30 years, top researchers from all over the world have come to Austria in the framework of the "Alexander von Humboldt Colloquium" in order to discuss recent topics in astronomy and space physics. Christoph Lhotka organized this year's conference, chaired by IWF and University of Vienna, took place in Bad Hofgastein, Salzburg, from 19 to 25 March.

From 24 to 26 July, the institute hosted the 5th *CHEOPS* Science Workshop at Schloss Seggau. The workshop, which saw 89 international participants, aimed at bringing together the community interested in the mission, providing information about its current status and preparing its scientific exploitation. The workshop was organized by Luca Fossati, in collaboration with the IWF exoplanet team.

Wolfgang Baumjohann served as Vice Director and chair of the Program Committee of the Summer School Alpbach, which took place from 18 to 27 July and was dedicated to "The Dusty Universe". Every year, 60 students and about 25 lecturers and tutors from among ESA's member states are invited to this meeting.

In addition, M.Y. Boudjada, G. Fischer, G. Kargl, M. Lendl, C. Möstl, and R. Nakamura were members of scientific program and/or organizing committees at three international conferences and/or workshops.

LECTURING

In summer 2017 and in winter term 2017/2018 IWF members gave lectures at the University of Graz, Graz University of Technology, University of Vienna, TU Braunschweig, FH Joanneum, and FH Wiener Neustadt.

THESES

Besides lecturing, members of the institute are supervising Bachelor, Diploma, Master and Doctoral Theses. In 2017, the following supervised theses have been completed:

Ritter, S.: Simulation und Analyse von Laser Entfernungsmessungen zur dynamischen Bahnbestimmung für den Anwendungsfall Space Debris, Master Thesis, Technische Universität Graz, 86 pages (2017)

Romero Lopera, J.: Statistical Analysis of Flux Ropes in the Plasma Sheet of the Magnetotail, Master Thesis, Technische Universität Graz, 130 pages (2017)

Weber, C.: Investigation of Exoplanetary Radio Emission: New Aspects in the Search for Exoplanets at Radio Wavelengths, Doctoral Thesis, Universität Graz, 239 pages (2017)

MENTORING

In the framework of the ÖAW mentoring system, organized by the Working Group on Non-Discrimination of ÖAW, Martin Volwerk served as mentor and one member of IWF participated as mentee (Fig. 43).

Fig. 43: Eberhard Widmann, director of the Stefan Meyer Institute of ÖAW, IWF researcher Monika Lendl, and Barbara Haberl, chair of the Working Group on Non-Discrimination, at the closing ceremony of the first mentoring program (© ÖAW/Elia Zilberberg).

PUBLICATIONS

REFEREED ARTICLES

Amerstorfer, U.V., H. Gröller, H. Lichtenegger, H. Lammer, F. Tian, L. Noack, M. Scherf, C. Johnstone, L. Tu, M. Güdel: Escape and evolution of Mars's CO_2 atmosphere: Influence of suprathermal atoms, *J. Geophys. Res.*, **122**, 1321-1337 (2017)

Ammler-Von Eiff, M., E.W. Guenther: On the optimum operating conditions of ThNe calibration lamps for measurements of radial velocity variations, *Astron. Nachr.*, **338**, 550-583 (2017)

Antunes Tambara, L., J. Tonfat, A. Santos, F. Lima Kastensmidt, N.H. Medina, N. Added, V.A.P. Aguiar, F. Aguirre, M.A.G. Silveira: Analyzing reliability and performance trade-offs of HLS-based designs in SRAM-based FPGAs under soft errors, *IEEE Trans. Nucl. Sci.*, **64**, 874-881 (2017)

Aplin, K.L., G. Fischer: Lightning detection in planetary atmospheres, *Weather*, **72**, 46-50 (2017)

Bagashvili, S.R., B.M. Shergelashvili, D.R. Japaridze, B.B. Chargeishvili, A.G. Kosovichev, V. Kukhianidze, G. Ramishvili, T.V. Zaqarashvili, S. Poedts, M.L. Khodachenko, P. De Causmaecker: Statistical properties of coronal hole rotation rates: Are they linked to the solar interior?, *Astron. Astrophys.*, **603**, A134 (2017)

Barros, S.C.C., H. Gosselin, J. Lillo-Box, D. Bayliss, E. Delgado Mena, B. Brugger, A. Santerne, D.J. Armstrong, V. Adibekyan, J.D. Armstrong, D. Barrado, J. Bento, I. Boisse, A.S. Bonomo, F. Bouchy, D.J.A. Brown, W.D. Cochran, A. Collier Cameron, M. Deleui, O. Demangeon, R.F. Díaz, A. Doyle, X. Dumusque, D. Ehrenreich, N. Espinoza, F. Faedi, J.P. Faria, P. Figueira, E. Foxell, G. Hébrard, S. Hojjatpanah, J. Jackman, M. Lendl, R. Ligi, C. Lovis, C. Melo, O. Mousis, J.J. Neal, H.P. Osborn, D. Pollacco, N.C. Santos, R. Sefako, A. Shporer, S.G. Sousa, A.H.M.J. Triaud, S. Udry, A. Vigan, A. Wyttenbach: Precise masses for the transiting planetary system HD 106315 with HARPS, *Astron. Astrophys.*, **608**, A25 (2017)

Blum, J., B. Gundlach, M. Krause, M. Fulle, A. Johansen, J. Agarwa, I. von Borstel, X. Shi, X. Hu, M.S. Bentley, F. Capaccioni, L. Colangeli, V. Della Corte, N. Fougere, S.F. Green, S. Ivanovski, T. Mannel, S. Merouane, A. Migliorini, A. Rotundi, R. Schmied, C. Snodgrass: Evidence for the formation of comet 67P/Churyumov-Gerasimenko through gravitational collapse of a bound clump of pebbles, *MNRAS*, **469**, S755-S773 (2017)

Boetticher, A. von, A.H.M.J. Triaud, D. Queloz, S. Gill, M. Lendl, L. Delrez, D.R. Anderson, A. Collier Cameron, F. Faedi, M. Gillon, Y. Gómez Maqueo Chew, L. Hebb, C. Hellier, E. Jehin, P.F.L. Maxted, D.V. Martin, F. Pepe, D. Pollacco, D. Ségransan, B. Smalley, S. Udry, R. West: The EBLM project. III. A Saturn-size low-mass star at the hydrogen-burning limit, *Astron. Astrophys.*, **604**, L6 (2017)

Boudjada, M.Y., P.F. Biagi, E. Al-Haddad, P.H.M. Galopeau, B.P. Besser, D. Wolbang, G. Prattes, H. Eichelberger, G. Stangl, M. Parrot, K. Schwingenschuh: Reception conditions of low frequency (LF) transmitter signals onboard DEMETER micro-satellite, *Phys. Chem. Earth*, **102**, 70-79 (2017)

Bourdin, P.-A.: Catalog of fine-structured electron velocity distribution functions - Part 1: Antiparallel magnetic-field reconnection (Geospace Environmental Modeling case), *Ann. Geophys.*, **35**, 1051-1067 (2017)

Bourdin, Ph.-A.: Plasma beta stratification in the solar atmosphere: A possible explanation for the penumbra formation, *Astrophys. J. Lett.*, **850**, L29 (2017)

Brown, D.J.A., A.H.M.J. Triaud, A.P. Doyle, M. Gillon, M. Lendl, D.R. Anderson, A. Collier Cameron, G. Hebrard, C. Hellier, C. Lovis, P.F.L. Maxted, F. Pepe, D. Pollacco, D. Queloz, B. Smalley: Rossiter-McLaughlin models and their effect on estimates of stellar rotation, illustrated using six WASP systems, *MNRAS*, **464**, 810-839 (2017)

Cabrera, J., S.C.C. Barros, D. Armstrong, D. Hidalgo, N.C. Santos, J.M. Almenara, R. Alonso, M. Deleuil, O. Demangeon, R.F. Díaz, M. Lendl, J. Pfaff, H. Rauer, A. Santerne, L.M. Serrano, S. Zucker: Disproving the validated planets K2-78b, K2-82b, and K2-92b. The importance of independently confirming planetary candidates, *Astron. Astrophys.*, **606**, A75 (2017)

Cassak, P.A., K.J. Genestreti, J.L. Burch, T.-D. Phan, M.A. Shay, M. Swisdak, J.F. Drake, L. Price, S. Eriksson, R.E Ergun, B.J. Anderson, V.G. Merkin, C.M. Komar: The effect of a guide field on local energy conversion during asymmetric magnetic reconnection: Particle-in-Cell simulations, *J. Geophys. Res.*, **122**, 11523-11542 (2017)

Castro, N., L. Fossati, S. Hubrig, S.P. Järvinen, N. Przybilla, M.-F. Nieva, I. Ilyin, T.A. Carroll, M. Schöller, N. Langer, F.R.N. Schneider, S. Simón.-Díaz, T. Morel, K. Butler, and the BOB collaboration: B field in OB stars (BOB): The outstandingly strong magnetic field in the evolved He-strong star CPD-62° 2124, *Astron. Astrophys.*, **597**, L6 (2017)

Chasapis, A., W.H. Matthaeus, T.N. Parashar, O. LeContel, A. Retinò, H. Breuillard, Y. Khotyaintsev, A. Vaivads, B. Lavraud, E. Eriksson, T.E. Moore, J.L. Burch, R.B. Torbert, P.-A. Lindqvist, R.E. Ergun, G. Marklund, K.A. Goodrich, F.D. Wilder, M. Chutter, J. Needell, D. Rau, I. Dors, C.T. Russell, G. Le, W. Magnes, R.J. Strangeway, K.R. Bromund, H.K. Leinweber, F. Plaschke, D. Fischer, B.J. Anderson, C.J. Pollock, B.L. Giles, W.R. Paterson, J. Dorelli, D.J. Gershman, L. Avanov, Y. Saito: Electron heating at kinetic scales in magnetosheath turbulence, *Astrophys. J.*, **836**, 247 (2017)

Chen, Y.Q., T.L. Zhang, S.D. Xiao, G.Q. Wang: Characteristics of ionospheric flux rope at the terminator observed by Venus Express, *J. Geophys. Res.*, **122**, 8858–8867 (2017)

Cherenkov, A., D. Bisikalo, L. Fossati, C. Möstl: The influence of Coronal Mass Ejections on the mass-loss rates of Hot-Jupiters, *Astrophys. J.*, **846**, 31 (2017)

Chiavassa, A., R. Norris, M. Montargès, R. Ligi, L. Fossati, L. Bigot, F. Baron, P. Kervella, J.D. Monnier, D. Mourard, N. Nardetto, G. Perrin, G.H. Schaefer, T.A. ten Brummelaar, Z. Magic, R. Collet, M. Asplund: Asymmetries on red giant branch surfaces from CHARA/MIRC optical interferometry, *Astron. Astrophys.*, **600**, L2 (2017)

Chong, G.S., S.A. Pope, T.L. Zhang, G.A. Collinson, S.N. Walker, M.A. Balikhin: A study of ionopause perturbation and associated boundary wave formation at Venus, *J. Geophys. Res.*, **122**, 4284-4298 (2017)

Cubillos, P., J. Harrington, T. Loredo, N.B. Lust, J. Blecic, M. Stemm: On correlated-noise analyses applied to exoplanet light curves, *Astron. J.*, **153**, 3 (2017)

Cubillos, P., N.V. Erkaev, I. Juvan, L. Fossati, C.P. Johnstone, H. Lammer, M. Lendl, P. Odert, K.G. Kislyakova: An overabundance of low-density Neptune-like planets, *MNRAS*, **466**, 1868-1879 (2017)

Cubillos, P.E.: An algorithm to compress line-transition data for radiative-transfer calculations, *Astrophys. J.*, **850**, 32 (2017)

Cubillos, P.E., L. Fossati, N.V. Erkaev, M. Malik, T. Tokano, M. Lendl, C.P. Johnstone, H. Lammer, A. Wyttenbach: Aerosol constraints on the atmosphere of the Hot Saturn-mass planet WASP-49b, *Astrophys. J.*, **849**, 145 (2017)

De Spiegeleer, A., M. Hamrin, T. Pitkänen, M. Volwerk, I. Mann, H. Nilsson, P. Norqvist, L. Andersson, J. Vaverka: Low-frequency oscillatory flow signatures and high-speed flows in the Earth's magnetotail, *J. Geophys. Res.*, **122**, 7042–7056 (2017)

Delva, M., M. Volwerk, R. Jarvinen, C. Bertucci: Asymmetries in the magnetosheath field draping on Venus' nightside, *J. Geophys. Res.*, **122**, 10396-10407 (2017)

Desai, R.T., M.M. Cowee, H. Wei, X. Fu, S.P. Gary, M. Volwerk, A.J. Coates: Hybrid simulations of positively and negatively charged pickup ions and cyclotron wave generation at Europa, *J. Geophys. Res.*, **122**, 10408-10420 (2017)

Dumbadze, G., B.M. Shergelashvili, V. Kukhianidze, G. Ramishvili, T.V. Zaqarashvili, M. Khodachenko, E. Gurgenashvili, S. Poedts, P. De Causmaecker: Long-period oscillations of active region patterns: Least-squares mapping on second-order curves, *Astron. Astrophys.*, **597**, A93 (2017)

Dwivedi, N.K., S. Singh: Inertial range spectrum of field-aligned whistler turbulence, *Phys. Scripta*, **92**, 035001 (2017)

Dwivedi, N.K., S. Singh: Nonlinear whistler wave model for lion roars in the Earth's magnetosheath, *Astrophys. Space Sci.*, **362**, 172 (2017)

Dyadechkin, S., V.S. Semenov, E. Kallio, N.V. Erkaev, M. Alho, H. Lammer: Global kinetic hybrid simulation for radially expanding solar wind, *J. Geophys. Res.*, **122**, 7854-7864 (2017)

Eastwood, J.P., R. Nakamura, L. Turc, L. Mejnertsen, M. Hesse: The scientific foundations of forecasting magnetospheric space weather, *Space Sci. Rev.*, **212**, 1221-1252 (2017)

Ellerbroek, L., B. Gundlach, A. Landeck, C. Dominik, J. Blum, S. Merouane, M. Hilchenbach, M.S. Bentley, T. Mannel, H. John, H.A. van Veen: The footprint of cometary dust analogs: I. Laboratory experiments of low-velocity impacts and comparison with Rosetta data, *MNRAS*, **469**, S204–S216 (2017)

Ergun, R.E., L.-J. Chen, F.D. Wilder, N. Ahmadi, S. Eriksson, M.E. Usanova, K.A. Goodrich, J.C. Holmes, A.P. Sturner, D.M. Malaspina, D.L. Newman, R.B. Torbert, M.R. Argall, P.-A. Lindqvist, J.L. Burch, J.M. Webster, J.F. Drake, L. Price, P.A. Cassak, M. Swisdak, M.A. Shay, D.B. Graham, R.J. Strangeway, C.T. Russell, B.L. Giles, J.C. Dorelli, D. Gershman, L. Avanov, M. Hesse, B. Lavraud, O. Le Contel, A. Retino, T.D. Phan, M.V. Goldman, J.E. Stawarz, S.J. Schwartz, J.P. Eastwood, K.-J. Hwang, R. Nakamura, S. Wang: Drift waves, intense parallel electric fields, and turbulence associated with asymmetric magnetic reconnection at the magnetopause, *Geophys. Res. Lett.*, **44**, 2978-2986 (2017)

Erkaev, N.V., P. Odert, H. Lammer, K.G. Kislyakova, L. Fossati, A.V. Mezentsev, C.P. Johnstone, D.I. Kubyshkina, I.F. Shaikhislamov, M.L. Khodachenko: Effect of stellar wind induced magnetic fields on planetary obstacles of non-magnetized hot Jupiters, *MNRAS*, **470**, 4330-4336 (2017)

Fossati, L., N.V. Erkaev, H. Lammer, P.E. Cubillos, P. Odert, I. Juvan, K.G. Kislyakova, M. Lendl, D. Kubyshkina, S.J. Bauer: Aeronomical constraints to the minimum mass and maximum radius of hot low-mass planets, *Astron. Astrophys.*, **598**, A90 (2017)

Fossati, L., S.E. Marcelja, D. Staab, P.E. Cubillos, K. France, C.A. Haswell, S. Ingrassia, J.S. Jenkins, T. Koskinen, A.F. Lanza, S. Redfield, A. Youngblood, G. Pelzmann: The effect of ISM absorption on stellar activity measurements and its relevance for exoplanet studies, *Astron. Astrophys.*, **601**, A104 (2017)

Fränz, M., E. Echer, A. Marques de Souza, E. Dubinin, T.L. Zhang: Ultra low frequency waves at Venus: Observations by the Venus Express spacecraft, *Planet. Space Sci.*, **146**, 55-65 (2017)

Friedrich, M., C. Pock, K. Torkar: Long-term trends in the D- and E-region based on rocket-borne measurements, *J. Atmos. Sol.-Terr. Phys.*, **163**, 78-84 (2017)

Frühauff, D., F. Plaschke, K.-H. Glassmeier: Spin axis offset calibration on THEMIS using mirror modes, *Ann. Geophys.*, **35**, 117-121 (2017)

Fuselier, S.A., J.L. Burch, J. Mukherjee, K.J. Genestreti, S.K. Vines, R. Gomez, J. Goldstein, K.J. Trattner, S.M. Petrinec, B. Lavraud, R.J. Strangeway: Magnetospheric ion influence at the dayside magnetopause, *J. Geophys. Res.*, **122**, 8617-8631 (2017)

Gandolfi, D., O. Barragán, A.P. Hatzes, M. Fridlund, L. Fossati, P. Donati, M.C. Johnson, G. Nowak, J. Prieto-Arranz, S. Albrecht, F. Dai, H. Deeg, M. Endl, S. Grziwa, M. Hjorth, J. Korth, D. Nespra, J. Saario, A.M.S. Smith, G. Antoniciello, J. Alarcon, M. Bedell, P. Blay, S.S. Brems, J. Cabrera, S. Csizmadia, F. Cusano, W.D. Cochran, P. Eigmüller, A. Erikson, J.I. González Hernández, E.W. Guenther, T. Hirano, A. Suárez Mascareño, N. Narita, E. Palle, H. Parviainen, M. Pätzold, C.M. Persson, H. Rauer, I. Saviane, L. Schmidtobreick, V. Van Eylen, J.N. Winn, O.V. Zakhozhay: The transiting multi-planet system HD3167: A 5.7 M⊕ Super-Earth and an 8.3 M⊕ Mini-Neptune, *Astron. J.*, **154**, 123 (2017)

Genestreti, K.J., J. Goldstein, G.D. Corley, W. Farner, L.M. Kistler, B.A. Larsen, C.G. Mouikis, C. Ramnarace, R.M. Skoug, N.E. Turner: Temperature of the plasmasphere from Van Allen Probes HOPE, *J. Geophys. Res.*, **122**, 310-323 (2017)

Genestreti, K.J., J.L. Burch, P.A. Cassak, R.B. Torbert, R.E. Ergun, A. Varsani, T.D. Phan, B.L. Giles, C.T. Russell, S. Wang, M. Akhavan-Tafti, R.C. Allen: The effect of a guide field on local energy conversion during asymmetric magnetic reconnection: MMS observations, *J. Geophys. Res.*, **122**, 11342-11353 (2017)

Goetz, C., M. Volwerk, I. Richter, K.-H. Glassmeier: Evolution of the magnetic field at comet 67P/Churyumov-Gerasimenko, *MNRAS*, **469**, S268-S275 (2017)

Graham, D.B., Yu.V. Khotyaintsev, A. Vaivads, C. Norgren, M. André, J.M. Webster, J.L. Burch, P.-A. Lindqvist, R.E. Ergun, R.B. Torbert, W.R. Paterson, D.J. Gershman, B.L. Giles, W. Magnes, C.T. Russell: Instability of agyrotropic electron beams near the electron diffusion region, *Phys. Rev. Lett.*, **119**, 025101 (2017)

Graham, D.B., Yu.V. Khotyaintsev, C. Norgren, A. Vaivads, M. André, S. Toledo-Redondo, P.-A. Lindqvist, G.T. Marklund, R.E. Ergun, W.R. Paterson, D.J. Gershman, B.L. Giles, C.J. Pollock, J.C. Dorelli, L.A. Avanov, B. Lavraud, Y. Saito, W. Magnes, C.T. Russell, R.J. Strangeway, R.B. Torbert, J.L. Burch: Lower hybrid waves in the ion diffusion and magnetospheric inflow regions, *J. Geophys. Res.*, **122**, 517-533 (2017)

Guenther, E.W., O. Barragán, F. Dai, D. Gandolfi, T. Hirano, M. Fridlund, L. Fossati, A. Chau, R. Helled, J. Korth, J. Prieto-Arranz, D. Nespral, G. Antoniciello, H. Deeg, M. Hjorth, S. Grziwa, S. Albrecht, A.P. Hatzes, H. Rauer, Sz. Csizmadia, A.M.S. Smith, J. Cabrera, N. Narita, P. Arriagada, J. Burt, R.P. Butler, W.D. Cochran, J.D. Crane, Ph. Eigmüller, A. Erikson, J.A. Johnson, A. Kiilerich, D. Kubyshkina, E. Palle, C.M. Persson, M. Pätzold, S. Sabotta, B. Sato, St.A. Shectman, J.K. Teske, I.B. Thompson, V. Van Eylen, G. Nowak, A. Vanderburg, J.N. Winn, R.A. Wittenmyer: K2-106, a system containing a metal-rich planet and a planet of lower density, *Astron. Astrophys.*, **608**, A93 (2017)

Gurgenashvili, E., T.V. Zaqarashvili, V. Kukhianidze, R. Oliver, J.L. Ballester, M. Dikpati, S.W. McIntosh: North-south asymmetry in Rieger-type periodicity during solar cycles 19-23, *Astrophys. J.*, **845**, 137 (2017)

Gvaramadze, V.V., N. Langer, L. Fossati, D.C.-J. Bock, N. Castro, I.Y. Georgiev, J. Greiner, S. Johnston, A. Rau, T.M. Tauris: A solar-type star polluted by calcium-rich supernova ejecta inside the supernova remnant RCW 86, *Nat. Astron.*, **1**, 0116 (2017)

Hardy, R.A., J. Harrington, M.R. Hardin, N. Madhusudhan, T.J. Loredo, R.C. Challener, A.S.D. Foster, P.E. Cubillos, J. Blecic: Secondary eclipses of HAT-P-13b, *Astrophys. J.*, **836**, 143 (2017)

Hasegawa, H., B.U.Ö. Sonnerup, R.E. Denton, T.-D. Phan, T.K.M. Nakamura, B.L. Giles, D.J. Gershman, J.C. Dorelli, J.L. Burch, R.B. Torbert, C.T. Russell, R.J. Strangeway, P.-A. Lindqvist, Y.V. Khotyaintsev, R.E. Ergun, P.A. Cassak, N. Kitamura, Y. Saito: Reconstruction of the electron diffusion region observed by the Magnetospheric Multiscale spacecraft: First results, *Geophys. Res. Lett.*, **44**, 4566-4574 (2017)

Hellier, C., D.R. Anderson, A. Collier Cameron, L. Delrez, M. Gillon, E. Jehin, M. Lendl, P.F.L. Maxted, M. Neveu-VanMalle, F. Pepe, D. Pollacco, D. Queloz, D. Segransan, B. Smalley, J. Southworth, A.H.M.J. Triaud, S. Udry, T. Wagg, R.G. West: WASP-South transiting exoplanets: WASP-130b, WASP-131b, WASP-132b, WASP-139b, WASP-140b, WASP-141b and WASP-142b, *MNRAS*, **465**, 3693-3707 (2017)

Hilchenbach, M., H. Fischer, Y. Langevin, S. Merouane, J. Paquette, J. Rynö, O. Stenzel, C. Briois, J. Kissel, A. Koch, R. Schulz, J. Silen, N. Altobelli, D. Baklouti, A. Bardyn, H. Cottin, C. Engrand, N. Fray, G. Haerendel, H. Henkel, H. Höfner, K. Hornung, H. Lehto, E.M. Mellado, P. Modica, L. Le Roy, S. Siljeström, W. Steiger, L. Thirkel, R. Thomas, K. Torkar, K. Varmuza, B. Zaprudin, COSIMA team: Mechanical and electrostatic experiments with dust particles collected in the inner coma of comet 67P by COSIMA onboard Rosetta, *Phil. Trans. R. Soc. A*, **375**, 20160255 (2017)

Huang, S.Y., F. Sahraoui, Z.G. Yuan, J.S. He, J.S. Zhao, O. Le Contel, X.H. Deng, M. Zhou, H.S. Fu, Q.Q. Shi, B. Lavraud, Y. Pang, J. Yang, D.D. Wang, H.M. Li, X.D. Yu, C.J. Pollock, B.L. Giles, R.B. Torbert, C.T. Russell, K.A. Goodrich, D.J. Gershman, T.E. Moore, R.E. Ergun, Y.V. Khotyaintsev, P.-A. Lindqvist, R.J. Strangeway, W. Magnes, K. Bromund, H. Leinweber, F. Plaschke, B.J. Anderson, J.L. Burch: Magnetospheric Multiscale observations of electron vortex magnetic hole in the turbulent magnetosheath plasma, *Astrophys. J. Lett.*, **836**, L27 (2017)

Khodachenko, M.L., I.F. Shaikhislamov, H. Lammer, K.G. Kislyakova, L. Fossati, C.P. Johnstone, O.V. Arkhypov, A.G. Berezutsky, I.B. Miroshnichenko, V.G. Posukh: Lyα

absorption at transits of HD 209458b: A comparative study of various mechanisms under different conditions, *Astrophys. J.*, **847**, 126 (2017)

Khutsishvili, D., T.V. Zaqarashvili, E. Khutsishvili, T. Kvernadze, V. Kulidzanishvili, V. Kakhiani, M. Sikharulidze: Anti-phase oscillations of Hα line Doppler velocity and width in solar limb spicules, *Astrophys. Space Sci.*, **362**, 235 (2017)

Kiehas, S.A., N.N. Volkonskaya, V.S. Semenov, N.V. Erkaev, I.V. Kubyshkin, I.V. Zaitsev: Large-scale energy budget of impulsive magnetic reconnection: Theory and simulation, *J. Geophys. Res.*, **122**, 3212-3231 (2017)

Kislyakova, K.G., L. Noack, C.P. Johnstone, V.V. Zaitsev, L. Fossati, H. Lammer, M.L. Khodachenko, P. Odert, M. Güdel: Magma oceans and enhanced volcanism on TRAPPIST-1 planets due to induction heating, *Nat. Astron.*, **1**, 878-885 (2017)

Kömle, N., C. Pitcher, Y. Gao, L. Richter: Study of the formation of duricrusts on the martian surface and their effect on sampling equipment, *Icarus*, **281**, 220-227 (2017)

Kömle, N.I., W. Macher, P. Tiefenbacher, G. Kargl, I. Pelivan, J. Knollenberg, T. Spohn, L. Jorda, C. Capanna, V. Lommatsch, B. Cozzoni, F. Finke: Three-dimensional illumination and thermal model of the Abydos region on comet 67P/Churyumov-Gerasimenko, *MNRAS*, **469**, S2-S19 (2017)

Kucharski, D., G. Kirchner, J. C. Bennett, M. Lachut, K. Sośnica, N. Koshkin, L. Shakun, F. Koidl, M. Steindorfer, P. Wang, C. Fan, X. Han, L. Grunwaldt, M. Wilkinson, J. Rodríguez, G. Bianco, F. Vespe, M. Catalán, K. Salmins, J. R. del Pino, H.-C. Lim, E. Park, C. Moore, P. Lejba, T. Suchodolski: Photon pressure force on space debris TOPEX/Poseidon measured by Satellite Laser Ranging: Spin-up of Topex, *Earth Space Sci.*, **4**, 661-668 (2017)

Kuridze, D., V. Henriques, M. Mathioudakis, J. Koza, T.V. Zaqarashvili, J. Rybák, A. Hanslmeier, F.P. Keenan: Spectroscopic inversions of the Ca II 8542 Å line in a C-class solar flare, *Astrophys. J.*, **846**, 9 (2017)

Kurth, W.S., G.B. Hospodarsky, D.L. Kirchner, B.T. Mokrzycki, T.F. Averkamp, W.T. Robison, C.W. Piker, M. Sampl, P. Zarka: The Juno Waves investigation, *Space Sci. Rev.*, **213**, 347-392 (2017)

Kuzma, B., K. Murawski, T.V. Zaqarashvili, P. Konkol, A. Mignone: Numerical simulations of solar spicules: Adiabatic and non-adiabatic studies, *Astron. Astrophys.*, **597**, A133 (2017)

Lam, K.W.F., F. Faedi, D.J.A. Brown, D.R. Anderson, L. Delrez, M. Gillon, G. Hébrard, M. Lendl, L. Mancini, J. Southworth, B. Smalley, A.H.M. Triaud, O.D. Turner, K.L. Hay, D.J. Armstrong, S.C.C. Barros, A.S. Bonomo, F. Bouchy, P. Boumis, A. Collier Cameron, A.P. Doyle, C. Hellier, T. Henning, E. Jehin, G. King, J. Kirk, T. Louden, P.F.L. Maxted, J.J. McCormac, H.P. Osborn, E. Palle, F. Pepe, D. Pollacco, J. Prieto-Arranz, D. Queloz, J. Rey, D. Ségransan, S. Udry, S. Walker, R.G. West, P.J. Wheatley: From dense hot Jupiter to low-density Neptune: The discovery of WASP-127b, WASP-136b, and WASP-138b, *Astron. Astrophys.*, **599**, A3 (2017)

Le Contel, O., R. Nakamura, H. Breuillard, M.R. Argall, D.B. Graham, D. Fischer, A. Retinò, M. Berthomier, R. Pottelette, L. Mirioni, T. Chust, F.D. Wilder, D.J. Gershman, A. Varsani, P.-A. Lindqvist, Yu.V. Khotyaintsev, C. Norgren, R.E. Ergun, K.A. Goodrich, J.L. Burch, R.B. Torbert, J. Needell, M. Chutter, D. Rau, I. Dors, C.T. Russell, W. Magnes, R.J. Strangeway, K.R. Bromund, H.Y. Wei, F. Plaschke, B.J. Anderson, G. Le, T.E. Moore, B.L. Giles, W.R. Paterson, C.J. Pollock, J.C. Dorelli, L.A. Avanov, Y. Saito, B. Lavraud, S.A. Fuselier, B.H. Mauk, I.J. Cohen, D.L. Turner, J.F. Fennell, T. Leonard, A.N. Jaynes: Lower hybrid drift waves and electromagnetic electron space-ohase holes associated with dipolarization fronts and field-aligned currents observed by the Magnetospheric Multiscale mission during a substorm, *J. Geophys. Res.*, **122**, 12236-12257 (2017)

Le, G., P.J. Chi, R.J. Strangeway, C.T. Russell, J.A. Slavin, K. Takahashi, H.J. Singer, B.J. Anderson, K. Bromund, D. Fischer, E.L. Kepko, W. Magnes, R. Nakamura, F. Plaschke, R.B. Torbert: Global observations of magnetospheric high-m poloidal waves during the 22 June 2015 magnetic storm, *Geophys. Res. Lett.*, **44**, 3456-3464 (2017)

Leitner, P., B. Lemmerer, A. Hanslmeier, T. Zaqarashvili, A. Veronig, H. Grimm-Strele, H.J. Muthsam: Structure of the solar photosphere studied from the radiation hydrodynamics code ANTARES, *Astrophys. Space Sci.*, **362**, 181 (2017)

Lendl, M., D. Ehrenreich, O.D. Turner, D. Bayliss, S. Blanco-Cuaresma, H. Giles, F. Bouchy, M. Marmier, S. Udry: Ground-based photometry of the 21-day Neptune HD106315c, *Astron. Astrophys.*, **603**, L5 (2017)

Lendl, M., P.E. Cubillos, J. Hagelberg, A. Müller, I. Juvan, L. Fossati: Signs of strong Na and K absorption in the transmission spectrum of WASP-103b, *Astron. Astrophys.*, **606**, A18 (2017)

Lhotka, C.: Steady state obliquity of a rigid body in the spin-orbit resonant problem: Application to Mercury, *Cel. Mech. Dyn. Astron.*, **129**, 397-414 (2017)

Li, J., J. Bortnik, W. Li, Q. Ma, R.M. Thorne, C.A. Kletzing, W.S. Kurth, G.B. Hospodarsky, J. Wygant, A. Breneman, S. Thaller, H.O. Funsten, D.G. Mitchel, J.W. Manweiler, R.B. Torbert, O. Le Contel, R.E. Ergun, P.-A. Lindqvist, K. Torkar, R. Nakamura, M. Andriopoulou, C.T. Russell: "Zipper-like" periodic magnetosonic waves: Van Allen Probes, THEMIS, and magnetospheric multiscale observations, *J. Geophys. Res.*, **122**, 1600-1610 (2017)

Liu, C., X. Feng, R. Nakamura, J. Guo, R. Wang: Double-peaked core field of flux ropes during magnetic reconnection, *J. Geophys. Res.*, **122**, 6374–6384 (2017)

Liu, J., V. Angelopoulos, X.-J. Zhang, A. Runov, A. Artemyev, F. Plaschke, S. Fu, S. Lu, Y.-H. Liu, X. Chu: Ultralow frequency waves deep inside the inner magnetosphere driven by dipolarizing flux bundles, *J. Geophys. Res.*, **122**, 10112-10128 (2017)

Liu, J.K., Y.S. Ge, T.L. Zhang: The statistical analysis on magnetic holes inside the Earth magnetotail plasma sheet (in Chinese), *Chin. J. Geophys.*, **60**, 873-878 (2017)

Lu, H., Y. Li, J. Cao, Y. Ge, T.L. Zhang, Y. Yu: Numerical simulation on the multiple dipolarization fronts in the magnetotail, *Phys. Plasmas*, **24**, 102903 (2017)

Martin, A.J., M.J. Stift, L. Fossati, S. Bagnulo, C. Scalia, F. Leone, B. Smalley: A spectroscopic study of the open cluster NGC 6250, *MNRAS*, **466**, 613-627 (2017)

Möstl, C., A. Isavnin, P.D. Boakes, E.K.J. Kilpua, J.A. Davies, R.A. Harrison, D. Barnes, V. Krupar, J.P. Eastwood, S.W. Good, R.J. Forsyth, V. Bothmer, M.A. Reiss, T. Amerstorfer, R.M. Winslow, B.J. Anderson, L.C. Philpott, L. Rodriguez, A.P. Rouillard, P. Gallagher, T. Nieves-Chinchilla, T.L. Zhang: Modeling observations of solar coronal mass ejections with heliospheric imagers verified with the Heliophysics System Observatory, *Space Weather*, **15**, 955-970 (2017)

Nakamura, R., K. Torkar, M. Andriopoulou, H. Jeszenszky, C.P. Escoubet, F. Cipriani, P.A. Lindqvist, S.A. Fuselier, C.J. Pollock, B.L. Giles, Y. Khotyaintsev: Initial results from the Active Spacecraft POtential Control onboard Magnetospheric MultiScale mission, *IEEE Trans. Plasma Sci.*, **45**, 1847-1852 (2017)

Nakamura, R., T. Nagai, J. Birn, V.A. Sergeev, O. Le Contel, A. Varsani, W. Baumjohann, T.K.M. Nakamura, S. Apatenkov, A. Artemyev, R.E. Ergun, S.A. Fuselier, D.J. Gershman, B.J. Giles, Yu.V. Khotyaintsev, P.-A. Lindqvist, W. Magnes, B. Mauk, C.T. Russell, H.J. Singer, J. Stawarz, R.J. Strangeway, B. Anderson, K.R. Bromund, D. Fischer, L. Kepko, G. Le, F. Plaschke, J.A. Slavin, I. Cohen, A. Jaynes, D.L. Turner: Near-Earth plasma sheet boundary dynamics during substorm dipolarization, *Earth Planets Space*, **69**, 129 (2017)

Nakamura, T.K.M., H. Hasegawa, W. Daughton, S. Eriksson, W.Y. Li, R. Nakamura: Turbulent mass transfer caused by vortex induced reconnection in collisionless magnetospheric plasmas, *Nat. Comm.*, **8**, 1582 (2017)

Nakamura, T.K.M., S. Eriksson, H. Hasegawa, S. Zenitani, W.Y. Li, K.J. Genestreti, R. Nakamura, W. Daughton: Mass and energy transfer across the Earth's magnetopause caused by vortex-induced reconnection, *J. Geophys. Res.*, **122**, 11505-11522 (2017)

Narita, Y.: Error estimate of Taylor's frozen-in flow hypothesis in the spectral domain, *Ann. Geophys.*, **35**, 325-331 (2017)

Narita, Y.: Review article: Wave analysis methods for space plasma experiment, *Nonlin. Proc. Geophys.*, **24**, 203-214 (2017)

Narita, Y.: Scaling laws of wave-cascading superfluid turbulence, *AIP Adv*, **7**, 065009 (2017)

Narita, Y.: Spectral moments for the analysis of frequency shift, broadening, and wavevector anisotropy in a turbulent flow, *Earth Planets Space*, **69**, 73 (2017)

Narita, Y., W. Motschmann: Ion-scale sideband waves and filament formation: Alfvénic impact on heliospheric plasma turbulence, *Front. Physics*, **5**, 8 (2017)

Narita, Y., Y. Nishimura, T. Hada: Minimum variance projection for direct measurements of power-law spectra in the wavenumber domain, *Ann. Geophys.*, **35**, 639-644 (2017)

Narita, Y., Z. Vörös: Lifetime estimate for plasma turbulence, *Nonlin. Proc. Geophys.*, **24**, 673-679 (2017)

Neiner, C., M.E. Oksala, C. Georgy, N. Przybilla, S. Mathis, G. Wade, M. Kondrak, L. Fossati, A. Blazere, B. Buysschaert, J. Grunhut: Discovery of magnetic A supergiants: The descendants of magnetic main-sequence B stars, *MNRAS*, **471**, 1926-1935 (2017)

Odert, P., M. Leitzinger, A. Hanslmeier, H. Lammer: Stellar coronal mass ejections - I. Estimating occurrence frequencies and mass-loss rates, *MNRAS*, **472**, 876-890 (2017)

Parunakian, S., S. Dyadechkin, I. Alexeev, E. Belenkaya, M. Khodachenko, E. Kallio, M. Alho: Simulation of Mercury's magnetosheath with a combined hybrid-paraboloid model, *J. Geophys. Res.*, **122**, 8310-8326 (2017)

Paunzen, E., G. Handler, M. Lendl, B. Baumann, C. Rab, S. Meingast, M. Rode-Paunzen, M. Netopil, V. Antoci, L. Zhu, M. Zejda, H. Bozi: Search for variables in six galactic open clusters, *New Astron.*, **52**, 133-139 (2017)

Philishvili, E., B.M. Shergelashvili, T.V. Zaqarashvili, V. Kukhianidze, G. Ramishvili, M. Khodachenko, S. Poedts, P. De Causmaecker: Quasi-oscillatory dynamics observed in ascending phase of the flare on March 6, 2012, *Astron. Astrophys.*, **600**, A67 (2017)

Plaschke, F., C. Goetz, M. Volwerk, I. Richter, D. Frühauff, Y. Narita, K.-H. Glassmeier, M.K. Dougherty: Fluxgate magnetometer offset vector determination by the 3D mirror mode method, *MNRAS*, **469**, S675-S684 (2017)

Plaschke, F., T. Karlsson, H. Hietala, M. Archer, Z. Vörös, R. Nakamura, W. Magnes, W. Baumjohann, R.B. Torbert, C.T. Russell, B.L. Giles: Magnetosheath high-speed jets: Internal structure and interaction with ambient plasma, *J. Geophys. Res.*, **122**, 10157-10175 (2017)

Poganski, J., H.F. Schweiger, G. Kargl, N.I. Kömle: DEM modelling of a dynamic penetration process on Mars as a part of the NASA InSight Mission, *Procedia Eng.*, **175**, 43-50 (2017)

Poganski, J., N.I. Kömle, G. Kargl, H.F. Schweiger, M. Grott, T. Spohn, O. Krömer, C. Krause, T. Wippermann, G. Tsakyridis, M. Fittock, R. Lichtenheldt, C. Vrettos, J.E. Andrade: Extended pile driving model to predict the penetration of the Insight/HP3 mole into the Martian soil, *Space Sci. Rev.*, **211**, 217-236 (2017)

Poh, G., J.A. Slavin, X. Jia, J.M. Raines, S.M. Imber, W.-J. Sun, D.J. Gershman, G.A. DiBraccio, K.J. Genestreti, A.W. Smith: Coupling between Mercury and its nightside magnetosphere: Cross-tail current sheet asymmetry and substorm current wedge formation, *J. Geophys. Res.*, **122**, 8419-8433 (2017)

Poh, G., J.A. Slavin, X. Jia, J.M. Raines, S.M. Imber, W.-J. Sun, D.J. Gershman, G.A. DiBraccio, K.J. Genestreti, A.W. Smith: Mercury's cross-tail current sheet: Structure, X-line location and stress balance, *Geophys. Res. Lett.*, **44**, 678-686 (2017)

Prochazka, I., J. Kodet, J. Blazej, G. Kirchner, F. Koidl, P. Wang: Identification and calibration of one-way delays in satellite laser ranging systems, *Adv. Space Res.*, **59**, 2466-2472 (2017)

Pylaev, O.S., T.V. Zaqarashvili, A.I. Brazhenko, V.N. Melnik, A. Hanslmeier, M. Panchenko: Oscillation of solar radio emission at coronal acoustic cut-off frequency, *Astron. Astrophys.*, **601**, A42 (2017)

Roberts, O.W., Y. Narita, C.P. Escoubet: Direct measurement of anisotropic and asymmetric wave vector spectrum in ion-scale solar wind turbulence, *Astrophys. J. Lett.*, **851**, L11 (2017)

Roberts, O.W., Y. Narita, X. Li, C.P. Escoubet, H. Laakso: Multipoint analysis of compressive fluctuations in the fast and slow solar wind, *J. Geophys. Res.*, **122**, 6940–6963 (2017)

Russell, C.T., R.J. Strangeway, C. Zhao, B.J. Anderson, W. Baumjohann, K.R. Bromund, D. Fischer, L. Kepko, G. Le, W. Magnes, R. Nakamura, F. Plaschke, J.A. Slavin, R.B. Torbert, T.E. Moore, W.R. Paterson, C.J. Pollock, J.L. Burch: Structure, force balance, and topology of Earth's magnetopause, *Science*, **356**, 960-963 (2017)

Sasunov, Yu.L., M.L. Khodachenko, I.I. Alexeev, E.S. Belenkaya, O.V. Mingalev, M.N. Melnik: The influence of kinetic effect on the MHD scalings of a thin current sheet, *J. Geophys. Res.*, **122**, 493-500 (2017)

Schneider, F.R.N., N. Castro, L. Fossati, N. Langer, A. de Koter: BONNSAI: Correlated stellar observables in Bayesian methods, *Astron. Astrophys.*, **598**, A60 (2017)

Schöller, M., S. Hubrig, L. Fossati, T.A. Carroll, M. Briquet, L.M. Oskinova, S. Järvinen, I. Ilyin, N. Castro, T. Morel, N. Langer, N. Przybilla, M.-F. Nieva, A.F. Kholtygin, H. Sana, A. Herrero, R.H. Barbá, A. de Koter, BOB Collaboration: B fields in OB stars (BOB): Concluding the FORS2 observing campaign, *Astron. Astrophys.*, **599**, A66 (2017)

Schreiber, R., M. Panchenko, J. Hanasz, R. Mutel, I. Christopher: Beaming of intense AKR seen from the Interball-2 spacecraft, *J. Geophys. Res.*, **122**, 249-257 (2017)

Sharifi, M.A., M.R. Seif, O. Baur, N. Sneeuw: Gravity field recovery from orbit information using the Lagrange formalism, *Ann. of Geophys.*, **60**, S0334 (2017)

Shi, J., Z. Zhang, K. Torkar, Z. Cheng, A. Fazakerley, M. Dunlop, C. Carr: Distribution of field-aligned electron events in the high-altitude polar region: Cluster observations, *J. Geophys. Res.*, **122**, 11245-11255 (2017)

Staab, D., C.A. Haswell, G.D. Smith, L. Fossati, J.R. Barnes, R. Busuttil, J.S. Jenkins: SALT observations of the chromospheric activity of transiting planet hosts: Mass-loss and star–planet interactions, *MNRAS*, **466**, 738-748 (2017)

Stawarz, J.E., J.P. Eastwood, A. Varsani, R.E. Ergun, M.A. Shay, R. Nakamura, T.D. Phan, J.L. Burch, D.J. Gershman, B.L. Giles, K.A. Goodrich, Y.V. Khotyaintsev, P.-A. Lindqvist, C.T. Russell, R.J. Strangeway, R.B. Torbert: Magnetospheric Multiscale analysis of intense field-aligned Poynting flux near the Earth's plasma sheet boundary, *Geophys. Res. Lett.*, **44**, 7106–7113 (2017)

Steindorfer, M.A., G. Kirchner, F. Koidl, P. Wang, A. Anton, J.Fernandez Sanchez, K. Merz: Stare and chase of space debris targets using real-time derived pointing data, *Adv. Space Res.*, **60**, 1201-1209 (2017)

Teh, W.-L., T.K.M. Nakamura, R. Nakamura, W. Baumjohann, C.T. Russell, C. Pollock, P.-A. Lindqvist, R.E. Ergun, J.L. Burch, R.B. Torbert, B.L. Giles: Evolution of a typical ion-scale magnetic flux rope caused by thermal pressure enhancement, *J. Geophys. Res.*, **122**, 2040-2050 (2017)

Temple, L.Y., C. Hellier, M.D. Albrow, D.R. Anderson, D. Bayliss, T.G. Beatty, A. Bieryla, D.J.A. Brown, P.A. Cargile, A. Collier Cameron, K.A. Collins, K.D. Colon, I.A. Curtis, G. D'Ago, L. Delrez, J. Eastman, B.S. Gaudi, M. Gillon, J. Gregorio, D. James, E. Jehin, M.D. Joner, J.F. Kielkopf, R.B. Kuhn, J. Labadie-Bartz, D.W. Latham, M. Lendl, M.B. Lund, A.L. Malpas, P.F.L. Maxted, G. Myers, T.E. Oberst, F. Pepe, J. Pepper, D. Pollacco, D. Queloz, J.E. Rodriguez, D. Segransan, R.J. Siverd, B. Smalley, K.G. Stassun, D.J. Stevens, C. Stockdale, T.G. Tan, A.H.M.J. Triaud, S. Udry, S.Jr. Villanueva, R.G. West, G. Zhou: WASP-167b/KELT-13b: Joint discovery of a hot Jupiter transiting a rapidly rotating F1V star, *MNRAS*, **471**, 2743–2752 (2017)

Tonfat, J., F. Lima Kastensmidt, L. Artola, G. Hubert, N.H. Medina, N. Added, V.A.P. Aguiar, F. Aguirre, E.L.A. Macchione, M.A.G. Silveira: Analyzing the influence of the angles of incidence and rotation on MBU events induced by low LET heavy ions in a 28-nm SRAM-based FPGA, *IEEE Trans. Nucl. Sci.*, **64**, 2161-2168 (2017)

Tonfat, J., L. Tambara, A. Santos, F.L. Kastensmidt: Soft error susceptibility analysis methodology of HLS designs in SRAM-based FPGAs, *Microproc. Microsyst.*, **51**, 209-219 (2017)

Torkar, K., R. Nakamura, M. Andriopoulou, B.L. Giles, H. Jeszenszky, Y.V. Khotyaintsev, P.-A. Lindqvist, R.B. Torbert: Influence of the ambient electric field on measurements of the actively controlled spacecraft potential by MMS, *J. Geophys. Res.*, **122**, 12019-12030 (2017)

Treumann, R.A., W. Baumjohann: Causal kinetic equation of non-equilibrium plasmas, *Ann. Geophys.*, **35**, 683-690 (2017)

Treumann, R.A., W. Baumjohann: Electron cyclotron maser instability (ECMI) in strong magnetic guide field reconnection, *Ann. Geophys.*, **35**, 999-1013 (2017)

Treumann, R.A., W. Baumjohann: The usefulness of Poynting's theorem in magnetic turbulence, *Ann. Geophys.*, **35**, 1353-1360 (2017)

Triaud, A.H.M.J., M. Neveu-VanMalle, M. Lendl, D.R. Anderson, A. Collier Cameron, L. Delrez, A. Doyle, M. Gillon, C. Hellier, E. Jehin, P.F.L. Maxted, D. Segransan, B.

Smalley, D. Queloz, D. Pollacco, J. Southworth, J. Tregloan-Reed, S. Udry, R. West: Peculiar architectures for the WASP-53 and WASP-81 planet-hosting systems, *MNRAS*, **467**, 1714-1733 (2017)

Varsani, A., R. Nakamura, V.A. Sergeev, W. Baumjohann, C.J. Owen, A.A. Petrukovich, Z. Yao, T.K.M. Nakamura, M.V. Kubyshkina, T. Sotirelis, J.L. Burch, K.J. Genestreti, Z. Vörös, M. Andriopoulou, D.J. Gershman, L.A. Avanov, W. Magnes , C.T. Russell, F. Plaschke, Y.V. Khotyaintsev, B.L. Giles, V.N. Coffey, J.C. Dorelli, R.J. Strangeway, R.B. Torbert, P.-A. Lindqvist, R. Ergun: Simultaneous remote observations of intense reconnection effects by DMSP and MMS spacecraft during a storm time substorm, *J. Geophys. Res.*, **122**, 10891-10909 (2017)

Volwerk, M., G.H. Jones, T. Broiles, J. Burch, C. Carr, A.J. Coates, E. Cupido, M. Delva, N.J.T. Edberg, A. Eriksson, C. Goetz, R. Goldstein, P. Henri, H. Madanian, H. Nilsson, I. Richter, K. Schwingenschuh, G. Stenberg Wieser, K.-H. Glassmeier: Current sheets in comet 67P/Churyumov-Gerasimenko's coma, *J. Geophys. Res.*, **122**, 3308-3321 (2017)

Vörös, Z., E. Yordanova, A. Varsani, K.J. Genestreti, Yu.V. Khotyaintsev, W. Li, D.B. Graham, C. Norgren, R. Nakamura, Y. Narita, F. Plaschke, W. Magnes, W. Baumjohann, D. Fischer, A. Vaivads, E. Eriksson, P.-A. Lindqvist, G. Marklund, R.E. Ergun, M. Leitner, M.P. Leubner, R.J. Strangeway, O. Le Contel, C. Pollock, B.J. Giles, R.B. Torbert, J.L. Burch, L.A. Avanov, J.C. Dorelli, D.J. Gershman, W.R. Paterson, B. Lavraud, Y. Saito: MMS observation of magnetic reconnection in the turbulent magnetosheath, *J. Geophys. Res.*, **122**, 11442-11467 (2017)

Wang, G.Q., M. Volwerk, T.L. Zhang, D. Schmid, A. Yoshikawa: High-latitude Pi2 pulsations associated with kink-like neutral sheet oscillations, *J. Geophys. Res.*, **122**, 2889-2899 (2017)

Wang, R., Q. Lu, R. Nakamura, W. Baumjohann, C.T. Russell, J.L. Burch, R.E. Ergun, P.A. Lindqvist, S. Wang, B. Giles, D. Gershman: Interaction of magnetic flux ropes via magnetic reconnection observed at the magnetopause, *J. Geophys. Res.*, **122**, 10436-10447 (2017)

Wang, R., R. Nakamura, Q. Lu, W. Baumjohann, R.E. Ergun, J.L. Burch, M. Volwerk, A. Varsani, T.K.M. Nakamura, W. Gonzalez, B. Giles, D. Gershman, S. Wang: Electron-scale quadrants of the Hall magnetic field observed by the Magnetospheric Multiscale spacecraft during asymmetric reconnection, *Phys. Rev. Lett.*, **118**, 175101 (2017)

Weber, C., H. Lammer, I.F. Shaikhislamov, J.M. Chadney, M.L. Khodachenko, J.-M. Grießmeier, H.O. Rucker, C. Vocks, W. Macher, P. Odert, K.G. Kislyakova: How expanded ionospheres of Hot Jupiters can prevent escape of radio emission generated by the cyclotron maser instability, *MNRAS*, **469**, 3505–3517 (2017)

Wei, Y., M. Fraenz, E. Dubinin, W. Wana, T. Zhang, Z. Rong, L. Chai, J. Zhong, R. Zhu, Y. Futaana, S. Barabash: Ablation of Venusian oxygen ions by unshocked solar wind, *Sci. Bull.*, **62**, 1669-1672 (2017)

Wilder, F.D., R.E. Ergun, D.L. Newman, K.A. Goodrich, K.J. Trattner, M.V. Goldman, S. Eriksson, A.N. Jaynes, T. Leonard, D.M. Malaspina, N. Ahmadi, S.J. Schwartz, J.L. Burch, R.B. Torbert, M.R. Argall, B.L. Giles, T.D. Phan, O. Le Contel, D.B. Graham, Yu.V. Khotyaintsev, R.J. Strangeway, C.T. Russell, W. Magnes, F. Plaschke, P.-A. Lindqvist: The nonlinear behavior of whistler waves at the reconnecting dayside magnetopause as observed by the Magnetospheric Multiscale mission: A case study, *J. Geophys. Res.*, **122**, 5487-5501 (2017)

Wilder, F.D., R.E. Ergun, S. Eriksson, T.D. Phan, J.L. Burch, N. Ahmadi, K.A. Goodrich, D.L. Newman, K.J. Trattner, R.B. Torbert, B.L. Giles, R.J. Strangeway, W. Magnes, P.-A. Lindqvist, Yu.V. Khotyaintsev: Multipoint measurements of the electron jet of symmetric magnetic reconnection with a moderate guide field, *Phys. Rev. Lett.*, **118**, 265101 (2017)

Wu, Q., A.M. Du, M. Volwerk, B.T. Tsurutani, Y.S. Ge: The distribution of oscillation frequency of magnetic field and plasma parameters in BBFs: THEMIS statistics, *J. Geophys. Res.*, **122**, 4325–4334 (2017)

Wurz, P., D. Lasi, N. Thomas, D. Piazza, A. Galli, M. Jutzi, S. Barabash, M. Wieser, W. Magnes, H. Lammer, U. Auster, L.I. Gurvits, W. Hajdas: An impacting descent probe for Europa and the other Galilean moons of Jupiter, *Earth Moon Planets*, **120**, 113-146 (2017)

Xiao, S., T.L. Zhang, G. Wang, M. Volwerk, Y. Ge, D. Schmid, R. Nakamura, W. Baumjohann, F. Plaschke: Occurrence rate of dipolarization fronts in the plasma sheet: Cluster observations, *Ann. Geophys.*, **35**, 1015-1022 (2017)

Xiao, S.D., T.L. Zhang, G.Q. Wang: Statistical study of low-frequency magnetic field fluctuations near Venus during the solar cycle, *J. Geophys. Res.*, **122**, 8409-8418 (2017)

Yao, Z.H., I.J. Rae, R.L. Guo, A.N. Fazakerley, C.J. Owen, R. Nakamura, W. Baumjohann, C.E.J. Watt, K.J. Hwang, B.L. Giles, C.T. Russell, R.B. Torbert, A. Varsani, H.S. Fu, Q.Q. Shi, X.-J. Zhang: A direct examination of the dynamics of dipolarization fronts using MMS, *J. Geophys. Res.*, **122**, 4335-4347 (2017)

Yushkov, E., A. Petrukovich, A. Artemyev, R. Nakamura: Relationship between electron field-aligned anisotropy and dawn-dusk magnetic field: Nine years of Cluster observations in the Earth magnetotail, *J. Geophys. Res.*, **122**, 9294-9305 (2017)

Zwintz, K., E. Moravveji, P.I. Pápics, A. Tkachenko, N. Przybilla, M.-F. Nieva, R. Kuschnig, V. Antoci, D. Lorenz, N. Themeßl, L. Fossati, T.G. Barnes: A comprehensive study of young B stars in NGC 2264. I. Space photometry and asteroseismology, *Astron. Astrophys.*, **601**, A101 (2017)

BOOKS

Fischer, G., G. Mann, M. Panchenko, P. Zarka (Eds.): Planetary Radio Emissions VIII. Proceedings of the 8th International Workshop on Planetary, Solar and Heliospheric Radio Emissions, Austrian Academy of Sciences Press, Vienna, 550 pages (2017)

PROCEEDINGS & BOOK CHAPTERS

Dorovskyy, V., V. Melnik, A. Konovalenko, A. Brazhenko, S. Poedts, H. Rucker, M. Panchenko: Properties of groups of solar S-bursts in the decameter band. In: *Planetary Radio Emissions VIII. Proc. of the 8th International Workshop on Planetary, Solar and Heliospheric Radio Emissions*, Eds. Fischer, G., G. Mann, M. Panchenko, P. Zarka, Austrian Academy of Sciences Press, Vienna, 369-378 (2017)

Fischer, G., B. Cecconi, J. Bergman, J. Girard, G. Quinsac, J.-E. Wahlund: Short antennas on a large spacecraft. In: *Planetary Radio Emissions VIII. Proc. of the 8th International Workshop on Planetary, Solar and Heliospheric Radio Emissions*, Eds. Fischer, G., G. Mann, M. Panchenko, P. Zarka, Austrian Academy of Sciences Press, Vienna, 515-523 (2017)

Fossati, L., K. France, B. Fleming, T. Koskinen, A. Vidotto, M. Beasley, J.-M. Desert, K. Hoadley, R. Kohnert, N. Nell, P. Petit: CUTE: The Colorado Ultraviolet Transit Experiment. In: *Proceedings of the Second BRITE-Constellation Science Conference - "Small Satellites - Big Science"*, Polish Astronomical Society, Warsaw, 73-75 (2017)

Hagen, C., M. Ellmeier, J. Piris, R. Lammegger, I. Jernej, W. Magnes, E. Murphy, A. Pollinger, C. Erd, W. Baumjohann: Long-term vacuun tests of single-mode vertical cavity surface emitting laser diodes used for a scalar magnetometer. In: *Proceedings Volume 10563, International Conference on Space Optics - ICSO 2014*, Eds. Z. Sodnik, B. Cugny, N. Karafolas, SPIE, Bellingham, WA, 105634Y (2017)

Konovalenko, A., P. Zarka, H.O. Rucker, V. Zakharenko, O. Ulyanov, M. Sidorchuk, S. Stepkin, V. Melnik, N. Kalinichenko, A. Stanislavsky, P. Tokarsky, V. Koliadin, V. Shepelev, V. Dorovskyy, I. Bubnov, S. Yerin, A. Reznichenko, G. Litvinenko, N. Shevchuk, A. Koval, I. Vasylieva, K. Mylostna, A. Skoryk, A. Shevtsova, Y. Volvach, E. Vasylkovsky, V. Ryabov, A. Lecacheux, L. Denis, M. Panchenko, G. Fischer, M. Imai, J.–M. Grießmeier, G.Mann, O. Litvinenko, A. Brazhenko, R. Vashchishin, A. Frantsuzenko, V. Koshovy, A. Lozinsky, O. Ivantyshin: Mulit-antenna observations in the low-frequency radio astronomy of solar system objects and re- lated topics studies. In: *Planetary Radio Emissions VIII. Proc. of the 8th International Workshop on Planetary, Solar and Heliospheric Radio Emissions*, Eds. Fischer, G., G. Mann, M. Panchenko, P. Zarka, Austrian Academy of Sciences Press, Vienna, 467-478 (2017)

Korhonen, H., K. Vida, M. Leitzinger, P. Odert, O.E. Kovacs: Hunting for stellar Coronal Mass Ejections. In: *Living around Active Stars (IAU S328). Proceedings of the International Astronomical Union Symposia and Colloquia*, Eds. Nandy, D., A. Valio, P. Petit, Cambridge University Press, Cambridge, 198-203 (2017)

Melnik, V. N., A.I. Brazhenko, G. Mann, A.A. Konovalenko, A.V. Frantsuzenko, H.O. Rucker, M. Panchenko: Radio manifestation of the CME observed on April 7, 2011 in the frequency band 8–32 MHz. In: *Planetary Radio Emissions VIII. Proc. of the 8th International Workshop on Planetary, Solar and Heliospheric Radio Emissions*, Eds. Fischer, G., G. Mann, M. Panchenko, P. Zarka, Austrian Academy of Sciences Press, Vienna, 381-390 (2017)

Mylostna, K.Y., V.V. Zakharenko, G. Fischer, A.A. Konovalenko, P. Zarka: Study of SED's emission parameters. In: *Planetary Radio Emissions VIII. Proc. of the 8th International Workshop on Planetary, Solar and Heliospheric Radio Emissions*, Eds. Fischer, G., G. Mann, M. Panchenko, P. Zarka, Austrian Academy of Sciences Press, Vienna, 223-231 (2017)

Panchenko, M., S. Rosker, H.O. Rucker, A. Brazhenko, A.A. Konovalenko, G. Litvinenko, P. Zarka, V. Melnik, V.E. Shaposhnikov, A.V. Frantsuzenko: Zebra-like fine spectral structures in Jovian decametric radio emission. In: *Planetary Radio Emissions VIII. Proc. of the 8th International Workshop on Planetary, Solar and Heliospheric Radio Emissions*, Eds. Fischer, G., G. Mann, M. Panchenko, P. Zarka, Austrian Academy of Sciences Press, Vienna, 103-115 (2017)

Scandariato, G., D. Ehrenreich, I. Pagano, D. Queloz, Y. Alibert, R. Alonso, T. Bárczy, D. Barrado y Novascués, W. Baumjohann, W. Benz, X. Bonfils, A. Brandeker, L. Borsato, C. Broeg, J. Cabrera, S. Charnoz, A.C. Cameron, M. Davies, O. Demangeon, M. Deleuil, A. Erikson, A. Fortier, L. Fossati, M. Fridlund, D. Gandolfi, M. Gillon, M. Güdel, A. Gutierrez Peña, K. Isaak, L. Kiss, J. Laskar, A. Lecavelier des Etangs, C. Lovis, M.R. Meyer, V. Nascimbeni, G. Oloffson, E. Pallé, G. Piotto, D. Pollacco, R. Ragazzoni, N. Rando, É. Renottes, I. Ribas, N.C. Santos, S. Sousa, T. Spohn, M. Steller, G. Szabó, N. Thomas, S. Udry, V. Van Grootel, N. Walton: CHEOPS (CHaracterising ExOPlanets Satellite) mission. In: *Proceedings of Science: Frontier Research in Astrophysics - II (PoS: FRAPWS2016)*, Proc. of Science, Trieste, 089 (2017)

Shi, J.K., Z. Wang, K. Torkar, G. Zherebtsov, K. Ratovsky, E. Nomanova: Study on plasma blob to result in radio signal scintillations in low latitude ionosphere. In: *Proceedings of the 2017 Progress In Electromagnetics Research Symposium - Spring (PIERS)*, IEEE, Piscataway, NJ, 2004-2007 (2017)

Steindorfer, M.A., G. Kirchner, F. Koidl, P. Wang: Space debris science at the satellite laser ranging station Graz. In: *Proceedings of the IEEE EEEIC International Conference on Environmental and Electrical Engineering 2017*, IEEE, Piscataway, NJ, 5 p. (2017)

Weber, C., H. Lammer, I.-F. Shaikhislamov, J.-M. Chadney, N. Erkaev, M.L. Khodachenko, J.-M. Grießmeier, H.O. Rucker, C. Vocks, W. Macher, P. Odert, K.G. Kislyakova: On the Cyclotron Maser Instability in magnetospheres of Hot Jupiters-influence of ionosphere models. In: *Planetary Radio Emissions VIII. Proc. of the 8th International Workshop on Planetary, Solar and Heliospheric Radio Emissions*, Eds. Fischer, G., G. Mann, M. Panchenko, P. Zarka, Austrian Academy of Sciences Press, Vienna, 317-329 (2017)

Ye, S.-Y., G. Fischer, W.S. Kurth, J.D. Menietti, D.A. Gurnett: Rotational modulation of Saturn Kilometric Radiation, narrrowband emission and auroral hiss. In: *Planetary Radio Emissions VIII. Proc. of the 8th International Workshop on Planetary, Solar and Heliospheric Radio Emissions*, Eds. Fischer, G., G. Mann, M. Panchenko, P. Zarka, Austrian Academy of Sciences Press, Vienna, 191-204 (2017)

For oral presentations and posters please refer to the "Publications" menu on www.iwf.oeaw.ac.at.

PERSONNEL

Agú, Martin A., Dipl.-Ing.
Aickara Gopinathan, Sreejith, Dr.
Al-Ubaidi, Tarek, Dipl.-Ing.
Almer, Hannes
Amerstorfer, Tanja, Dr.
Amerstorfer, Ute, Dr.
Arkhypov, Oleksiy, Dr.
Aydogar, Özer, Dipl.-Ing.
Baumjohann, Wolfgang, Prof.
Berghofer, Gerhard, Ing.
Besser, Bruno P., Dr.
Boakes, Peter D., Dr.
Boudjada, Mohammed Y., Dr.
Bourdin, Philippe, Dr.
Cubillos, Patricio, Dr.
Delva, Magda, Dr.
Dwivedi, Navin K., Dr.
Dyadechkin, Sergey A., Dr.
Ederle, Vincent
Eichelberger, Hans U., Dr.
Ellmeier, Michaela, Mag.
Fischer, David, Dipl.-Ing.
Fischer, Georg, Dr.
Flock, Barbara, Mag.
Fossati, Luca, Dr.
Fremuth, Gerhard, Dipl.-Ing.
Genestreti, Kevin J., Dr.
Giner, Franz, Dipl.-Ing.
Graf, Christian, Ing.
Gratzer, Alexander J.
Grill, Claudia
Hagen, Christian, Dipl.-Ing.
Hasiba, Johann, Dipl.-Ing.
Hofer, Bernhard, BSc
Hofmann, Karl, Dipl.-Ing.
Hofwimmer, Thomas, Ing.
Höck, Eduard, Dipl.-Ing.
Hradecky, Doris
Hummel, Fabian N.J.
Jernej, Irmgard, Ing.
Jeszenszky, Harald, Dipl.-Ing.
Juvan, Ines, Mag.
Kargl, Günter, Dr.
Khodachenko, Maxim L., Dr.
Kiehas, Stefan, Dr.
Kirchner, Georg, Dr.
Koidl, Franz, Ing.
Kömle, Norbert I., Doz.
Korovinskiy, Daniil, Dr.
Krauss, Sandro, Dr.
Kubyshkina, Daria, Dr.
Kürbisch, Christoph, Ing.
Laky, Gunter, Dipl.-Ing.
Lammer, Helmut, Dr.
Leichtfried, Mario, Ing.
Leitzinger, Martin, Dr.
Lendl, Monika, Dr.
Lhotka, Christoph, Dr.
Lichtenegger, Herbert I.M., Dr.
Macher, Wolfgang, Dr.
Magnes, Werner, Dr.
Mannel, Thurid, MSc
Močnik, Karl, Dr.
Möstl, Christian, Dr.
Muck, Cosima
Nakamura, Rumi, Doz.
Nakamura, Takuma, Dr.
Narita, Yasuhito, Doz.
Neukirchner, Sonja, Ing.
Nischelwitzer-Fennes, Ute, Ing.
Odert, Petra, Dr.
Ottacher, Harald, Dipl.-Ing.
Panchenko, Mykhaylo, Dr.
Panov, Evgeny, Dr.
Pitterle, Martin
Prattes, Gustav, Dipl.-Ing.
Reimond, Stefan, Dipl.-Ing.
Sasunov, Jury, Dr.
Scherf, Manuel, Mag.
Scherr, Alexandra, Mag.
Shergelashvili, Bidzina, Dr.
Stachel, Manfred, Dipl.-Ing.
Steinberger, Michael, Dipl.-Ing.
Steindorfer, Michael, Dr.
Steller, Manfred B., Dr.
Stieninger, Reinhard, Ing.
Sulis, Sophia, Dr.
Tiefenbacher, Patrick, Mag.
Tonfat Seclen, Jorge L., Dr.
Tschachler, Elvira, Mag.
Valavanoglou, Aris, Dipl.-Ing.
Voller, Wolfgang G., Mag.
Volwerk, Martin, Dr.
Wallner, Robert, Ing.
Wang, Peiyuan, Mag.
Wellenzohn, Simon
Wilfinger, Josef, BSc
Wirnsberger, Harald, Dipl.-Ing.
Zaqarashvili, Teimuraz, Dr.
Zhang, Tie-Long, Prof.

As of 31 December 2017

IMPRESSUM

PUBLISHER

Wolfgang Baumjohann, Director
Institut für Weltraumforschung (IWF)
Österreichische Akademie der Wissenschaften (ÖAW)
Schmiedlstraße 6, 8042 Graz, Austria
www.iwf.oeaw.ac.at

EDITORS

Bruno Besser, Alexandra Scherr, Martin Volwerk

DESIGN

Alexandra Scherr
pr.iwf@oeaw.ac.at
Twitter: @IWF_Graz

PRINT

Servicebetrieb ÖH-Uni Graz GmbH


ÖAW IWF